

Cosmology with the Sunyaev-Zel'dovich Effect

John E. Carlstrom¹, Gilbert P. Holder², and Erik D. Reese³

¹Center for Cosmological Physics, Department of Astronomy and Astrophysics, Department of Physics, Enrico Fermi Institute, University of Chicago, 5640 S. Ellis Avenue, Chicago, IL, 60637, email: jc@hyde.uchicago.edu

²Institute for Advanced Study, Princeton, NJ, 08540, email: holder@ias.edu

³Chandra Fellow, Department of Physics, University of California, Berkeley, CA, 94720, email: reese@cfpa.berkeley.edu

KEYWORDS: galaxy clusters, cosmic microwave background, structure formation, surveys

ABSTRACT: The Sunyaev-Zel'dovich effect (SZE) provides a unique way to map the large-scale structure of the universe as traced by massive clusters of galaxies. As a spectral distortion of the cosmic microwave background, the SZE is insensitive to the redshift of the galaxy cluster, making it well-suited for studies of clusters at all redshifts, and especially at reasonably high redshifts ($z > 1$) where the abundance of clusters is critically dependent on the underlying cosmology. Recent high signal-to-noise detections of the SZE have enabled interesting constraints on the Hubble constant and the matter density of the universe using small samples of galaxy clusters. Upcoming SZE surveys are expected to find hundreds to thousands of new galaxy clusters, with a mass selection function that is remarkably uniform with redshift. In this review we provide an overview of the SZE and its use for cosmological studies with emphasis on the cosmology that can, in principle, be extracted from SZE survey yields. We discuss the observational and theoretical challenges that must be met before precise cosmological constraints can be extracted from the survey yields.

1 INTRODUCTION

The Sunyaev-Zel'dovich Effect (SZE) offers a unique and powerful observational tool for cosmology. Recently, there has been considerable progress in detecting and imaging the SZE. Efforts over the first two decades after the SZE was first proposed in 1970 (Sunyaev & Zel'dovich 1970, 1972) yielded few reliable detections. Over the last decade, new detectors and observing techniques have allowed high quality detections and images of the effect for more than 50 clusters with redshifts as high as one. The next generation of SZE instruments that are now being built or planned will be orders of magnitude more efficient. Entering the

fourth decade of SZE observations, we are now in position to exploit fully the power of the SZE, by obtaining detailed images of a set of clusters to understand the intra-cluster medium (ICM), by obtaining large SZE samples of clusters to determine statistically robust estimates of the cosmological parameters and, most importantly, by conducting large untargeted SZE surveys to probe the high redshift universe. These surveys will provide a direct view of the growth of large scale structure and will provide large catalogs of clusters that extend past $z \sim 2$ with remarkably uniform selection functions.

The physics of the SZE has been covered well in previous reviews (Birkinshaw 1999; Rephaeli 1995; Sunyaev & Zel'dovich 1980a), with Birkinshaw (1999) and Carlstrom et al (2000) providing recent reviews of the observations. In this review, we look to the near future, using recent observations as a guide to what we can expect.

The SZE is best known for allowing the determination of cosmological parameters when combined with other observational diagnostics of clusters of galaxies such as X-ray emission from the intracluster gas, weak and strong lensing by the cluster potential, and optical galaxy velocity dispersion measurements. For example, cluster distances have been determined from the analysis of SZE and X-ray data, providing independent estimates of the Hubble constant. A large homogeneous sample of galaxy clusters extending to high redshift should allow a precise measure of this number, as well as a measure of the angular diameter distance relation to high redshift where it is highly sensitive to cosmological parameters. Similarly, the SZE and X-ray measurements will allow tight constraints on cluster gas mass fractions which can be used to estimate Ω_M assuming the composition of clusters represents a fair sample of the universal composition. The observed redshift dependence of the gas mass fraction can also be used to constrain cosmological parameters as well as test speculative theories of dark matter decay.

The most unique and powerful cosmological tool provided by the exploitation of the SZE will likely be the direct measurement of the evolution of the number density of galaxy clusters by deep, large scale SZE surveys. The redshift evolution of the cluster density is critically dependent on the underlying cosmology, and in principle can be used to determine the equation of state of the dark energy. SZE observations are particularly well suited for deep surveys because the important parameter that sets the detection limit for such a survey is the mass of the cluster; SZE surveys will be able to detect all clusters above a mass limit independent of the redshift of the clusters. This remarkable property of SZE surveys is due to the fact that the SZE is a distortion of the cosmic microwave background (CMB) spectrum. While the CMB suffers cosmological dimming with redshift, the ratio of the magnitude of the SZE to the CMB does not; it is a direct, redshift independent measurement of the ICM column density weighted by temperature, i.e., the pressure integrated along the line of sight. The total SZE flux detected will

be proportional to the total temperature-weighted mass (total integrated pressure) and, of course, inversely proportional to the square of the angular diameter distance. Adopting a reasonable cosmology and accounting for the increase in the universal matter density with redshift, the mass limit for a given SZE survey flux sensitivity is not expected to change more than a factor of $\sim 2 - 3$ for any clusters with $z > 0.05$.

SZE surveys therefore offer an ideal tool for determining the cluster density evolution. Analyses of even a modest survey covering ~ 10 square degrees will provide interesting constraints on the matter density of the universe. The precision with which cosmological constraints can be extracted from much larger surveys, however, will be limited by systematics due to our insufficient understanding of the structure of clusters, their gas properties and evolution.

Insights into the structure of clusters will be provided by high resolution SZE observations, especially when combined with other measurements of the clusters. Fortunately, many of the cluster properties derived directly from observational data can be determined in several different ways. For example, the gas mass fraction can be determined by various combinations of SZE, X-ray, and lensing observations. The electron temperature, a direct measure of a cluster's mass, can be measured directly through X-ray spectroscopy, or determined through the analysis of various combinations of X-ray, SZE, and lensing observations. Several of the desired properties of clusters are therefore over-constrained by observation, providing critical insights to our understanding of clusters, and critical tests of current models for the formation and evolution of galaxy clusters. With improved sensitivity, better angular resolution, and sources out to $z \sim 2$, the next generation of SZE observations will provide a good view of galaxy cluster structure and evolution. This will allow, in principle, the dependence of the cluster yields from large SZE surveys on the underlying cosmology to be separated from the dependence of the yields on cluster structure and evolution.

We outline the properties of the SZE in the next section and provide an overview of the current state of the observations in §3. This is followed in §4 by predictions for the expected yields of upcoming SZE surveys. In §5, we provide an overview of the cosmological tests which will be possible with catalogs of SZE-selected clusters. This is followed by a discussion of backgrounds, foregrounds, contaminants, and theoretical uncertainties that could adversely affect cosmological studies with the SZE and a discussion of observations which could reduce or eliminate these concerns. Throughout the paper, h is used to parametrize the Hubble constant by $H_0 = 100h \text{ km s}^{-1} \text{ Mpc}^{-1}$, and Ω_M and Ω_Λ are the matter density and vacuum energy density, respectively, in units of the critical density.

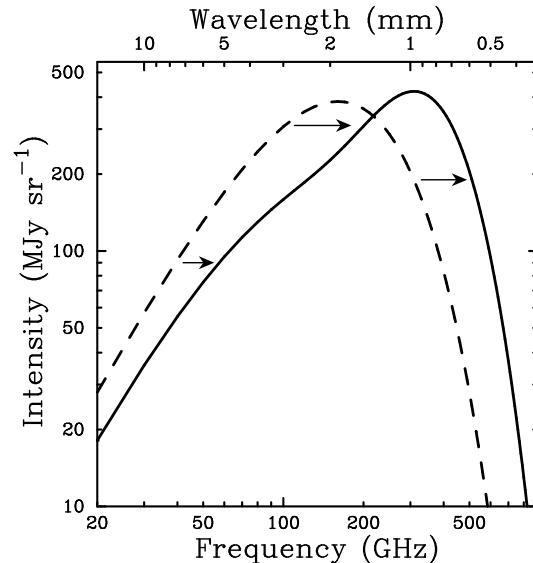


Figure 1: The Cosmic Microwave Background (CMB) spectrum, undistorted (dashed line) and distorted by the Sunyaev-Zel'dovich effect (SZE) (solid line). Following Sunyaev & Zel'dovich (1980a) to illustrate the effect, the SZE distortion shown is for a fictional cluster 1000 times more massive than a typical massive galaxy cluster. The SZE causes a decrease in the CMB intensity at frequencies $\lesssim 218$ GHz and an increase at higher frequencies.

2 THE SUNYAEV-ZEL'DOVICH EFFECT

2.1 Thermal Sunyaev-Zel'dovich Effect

The Sunyaev-Zel'dovich effect (SZE) is a small spectral distortion of the cosmic microwave background (CMB) spectrum caused by the scattering of the CMB photons off a distribution of high energy electrons. Here we focus only on the SZE caused by the hot thermal distribution of electrons provided by the intra-cluster medium (ICM) of galaxy clusters. CMB photons passing through the center of a massive cluster have only a $\approx 1\%$ probability of interacting with an energetic ICM electron. The resulting inverse Compton scattering preferentially boosts the energy of the CMB photon by roughly $k_B T_e / m_e c^2$ causing a small ($\lesssim 1$ mK) distortion in the CMB spectrum. Figure 1 shows the SZE spectral distortion for a fictional cluster that is over 1000 times more massive than a typical cluster to illustrate the small effect. The SZE appears as a decrease in the intensity of the

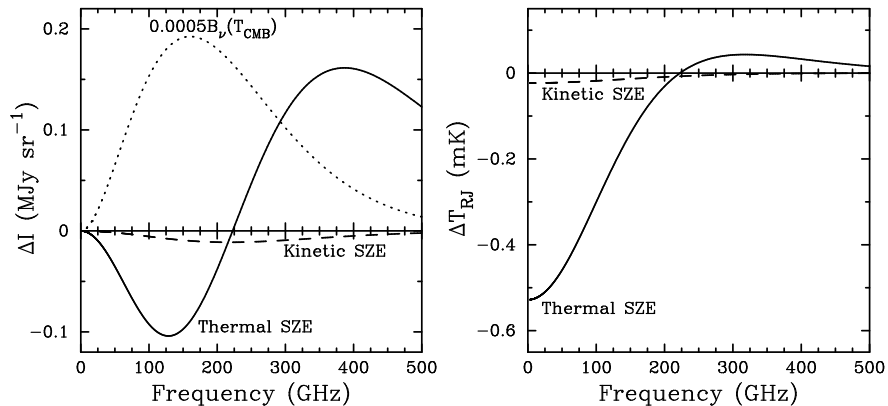


Figure 2: Spectral distortion of the cosmic microwave background (CMB) radiation due to the Sunyaev-Zel'dovich effect (SZE). The left panel shows the intensity and the right panel shows the Rayleigh Jeans brightness temperature. The thick solid line is the thermal SZE and the dashed line is the kinetic SZE. For reference the 2.7 K thermal spectrum for the CMB intensity scaled by 0.0005 is shown by the dotted line in the left panel. The cluster properties used to calculate the spectra are an electron temperature of 10 keV, a Compton y parameter of 10^{-4} , and a peculiar velocity of 500 km s^{-1} .

CMB at frequencies $\lesssim 218 \text{ GHz}$ and as an increase at higher frequencies.

The derivation of the SZE can be found in the original papers of Sunyaev and Zel'dovich (Sunyaev & Zel'dovich 1970, 1972), in several reviews (Sunyaev & Zel'dovich 1980a; Rephaeli 1995; Birkinshaw 1999), and in a number of more recent contributions which include relativistic corrections (see below for references). This review discusses the basic features of the SZE that make it a useful cosmological tool.

The SZE spectral distortion of the CMB expressed as a temperature change ΔT_{SZE} at dimensionless frequency $x \equiv \frac{h\nu}{k_B T_{CMB}}$ is given by

$$\frac{\Delta T_{SZE}}{T_{CMB}} = f(x) y = f(x) \int n_e \frac{k_B T_e}{m_e c^2} \sigma_T dl, \quad (1)$$

where y is the Compton y -parameter, which for an isothermal cluster equals the optical depth, τ_e , times the fractional energy gain per scattering, σ_T is the Thomson cross-section, n_e is the electron number density, T_e is the electron temperature, k_B is the Boltzmann constant, $m_e c^2$ is the electron rest mass energy, and the integration is along the line of sight. The frequency dependence of the

SZE is

$$f(x) = \left(x \frac{e^x + 1}{e^x - 1} - 4 \right) (1 + \delta_{SZE}(x, T_e)), \quad (2)$$

where $\delta_{SZE}(x, T_e)$ is the relativistic correction to the frequency dependence. Note that $f(x) \rightarrow -2$ in the non-relativistic and Rayleigh-Jeans (RJ) limits.

It is worth noting that $\Delta T_{SZE}/T_{CMB}$ is independent of redshift as shown in Eq. 1. This unique feature of the SZE makes it a potentially powerful tool for investigating the high redshift universe.

Expressed in units of specific intensity, common in millimeter SZE observations, the thermal SZE is

$$\Delta I_{SZE} = g(x) I_0 y, \quad (3)$$

where $I_0 = 2(k_B T_{CMB})^3 / (hc)^2$ and the frequency dependence is given by

$$g(x) = \frac{x^4 e^x}{(e^x - 1)^2} \left(x \frac{e^x + 1}{e^x - 1} - 4 \right) (1 + \delta_{SZE}(x, T_e)). \quad (4)$$

ΔT_{SZE} and ΔI_{SZE} are simply related by the derivative of the blackbody with respect to temperature, $|dB_\nu/dT|$.

The spectral distortion of the CMB spectrum by the thermal SZE is shown in Figure 2 (solid line) for a realistic massive cluster ($y = 10^{-4}$) in units of intensity (left panel) and Rayleigh-Jeans (RJ) brightness temperature (right panel). The RJ brightness is shown because the sensitivity of a radio telescope is calibrated in these units. It is defined simply by $I_\nu = (2k_B \nu^2 / c^2) T_{RJ}$ where I_ν is the intensity at frequency ν , k_B is Boltzmann's constant, and c is the speed of light. The CMB blackbody spectrum, $B_\nu(T_{CMB})$, multiplied by 0.0005 (dotted line) is also shown for comparison. Note that the spectral signature of the thermal effect is distinguished readily from a simple temperature fluctuation of the CMB. The kinetic SZE distortion is shown by the dashed curve (§2.2). In the non-relativistic regime, it is indistinguishable from a CMB temperature fluctuation.

The gas temperatures measured in massive galaxy clusters are around $k_B T_e \sim 10 \text{ keV}$ (Mushotzky & Scharf 1997; Allen & Fabian 1998) and are measured to be as high as $\sim 17 \text{ keV}$ in the galaxy cluster 1E 0657 – 56 (Tucker et al 1998). The mass is expected to scale with temperature roughly as $T_e \propto M^{2/3}$. At these temperatures, electron velocities are becoming relativistic and small corrections are required for accurate interpretation of the SZE. There has been considerable theoretical work to include relativistic corrections to the SZE (Wright 1979; Fabbri 1981; Rephaeli 1995; Rephaeli & Yankovitch 1997; Stebbins 1997; Itoh et al 1998; Challinor & Lasenby 1998; Sazonov & Sunyaev 1998a,b; Nozawa et al 1998b; Challinor & Lasenby 1999; Molnar & Birkinshaw 1999; Dolgov et al 2001). All of these derivations agree for $k_B T_e \lesssim 15 \text{ keV}$, appropriate for galaxy clusters. For a massive cluster with $k_B T_e \sim 10 \text{ keV}$ ($k_B T_e / m_e c^2 \sim 0.02$) the relativistic corrections to the SZE are of order a few percent in the RJ portion of the spectrum,

but can be substantial near the null of the thermal effect. Convenient analytical approximations to fifth order in $k_B T_e/m_e c^2$ are presented in Itoh et al (1998).

Particularly relevant for finding clusters with an SZE survey is the integrated SZE signal. Because the SZE signal is the integrated pressure, integrating over the solid angle of the cluster provides a sum of all of the electrons in the cluster weighted by temperature. This provides a relatively clean measure of the total thermal energy of the cluster. Integrating the SZE over the solid angle of the cluster, $d\Omega = dA/D_\lambda^2$, gives

$$\int \Delta T_{SZE} d\Omega \propto \frac{N_e \langle T_e \rangle}{D_\lambda^2} \propto \frac{M \langle T_e \rangle}{D_\lambda^2} \quad (5)$$

where N_e is the total number of electrons in the clusters, $\langle T_e \rangle$ is the mean electron temperature, D_λ is the angular diameter distance, and M is the mass of the cluster (either gas or total mass as $M_{gas} = M_{total} f_g$, where f_g is the gas mass fraction). The integrated SZE flux is simply the temperature weighted mass of the cluster divided by D_λ^2 . The angular diameter distance $D_\lambda(z)$ is fairly flat at high redshift. Also, a cluster of a given mass will be denser and therefore hotter at high redshift because the universal matter density increases as $(1+z)^3$. Therefore, one expects an SZE survey to detect all clusters above some mass threshold with little dependence on redshift (see §4.2).

The most important features of the thermal SZE are: 1) it is a small spectral distortion of the CMB of order ~ 1 mK, which is proportional to the cluster pressure integrated along the line of sight [Eq. 1]; 2) it is independent of redshift; 3) it has a unique spectral signature with a decrease in the CMB intensity at frequencies $\lesssim 218$ GHz and an increase at higher frequencies; and 4) the integrated SZE flux is proportional to the temperature weighted mass of the cluster (total thermal energy of the cluster) implying that SZE surveys will have a mass threshold nearly independent of redshift.

2.2 Kinetic Sunyaev-Zel'dovich Effect

If the cluster is moving with respect to the CMB rest frame there will be an additional spectral distortion due to the Doppler effect of the cluster bulk velocity on the scattered CMB photons. If a component of the cluster velocity, v_{pec} , is projected along the line of sight to the cluster, then the Doppler effect will lead to an observed distortion of the CMB spectrum referred to as the kinetic SZE. In the non-relativistic limit, the spectral signature of the kinetic SZE is a pure thermal distortion of magnitude

$$\frac{\Delta T_{SZE}}{T_{CMB}} = -\tau_e \left(\frac{v_{pec}}{c} \right), \quad (6)$$

where v_{pec} is along the line of sight; i.e., the emergent spectrum is still described completely by a Planck spectrum, but at a slightly different temperature, lower

(higher) for positive (negative) peculiar velocities (Sunyaev & Zel'dovich 1972; Phillips 1995; Birkinshaw 1999, see Figure 2).

Relativistic perturbations to the kinetic SZE are due to the Lorentz boost to the electrons provided by the bulk velocity (Nozawa et al 1998a; Sazonov & Sunyaev 1998a). The leading term is of order $(k_B T_e/m_e c^2)(v_{pec}/c)$ and for a 10 keV cluster moving at 1000 km s⁻¹ the effect is about an 8% correction to the non-relativistic term. The $(k_B T_e/m_e c^2)^2(v_{pec}/c)$ term is only about 1% of the non-relativistic kinetic SZE and the $(v_{pec}/c)^2$ term is only 0.2%.

2.3 Polarization of the Sunyaev-Zel'dovich Effect

The scattering of the CMB photons by the hot ICM electrons can result in polarization at levels proportional to powers of (v_{pec}/c) and τ_e . The largest polarization is expected from the anisotropic optical depth to a given location in the cluster. For example, toward the outskirts of a cluster one expects to see a concentric (radial) pattern of the linear polarization at frequencies where the thermal SZE is positive (negative). Plots of the polarization pattern are presented in Sazonov & Sunyaev (1999). Nonspherical morphology for the electron distributions will lead to considerably complicated polarization patterns. The peak polarization of this signal will be order τ_e times the SZE signal, i.e., of order $0.025(k_B T_e/m_e c^2)\tau_e^2$ times the CMB intensity. For a massive cluster with $\tau_e = 0.01$, the effect would be at the 0.1 μ K level toward the edge of the cluster. In principle, this effect could be used to measure the optical depth of the cluster and therefore separate T_e and τ_e from a measurement of the thermal SZE (see Eq. 1).

It can be shown that polarization of the SZE comes entirely from the quadrupole component of the local radiation field experienced by the scattering electron. In the case above, the quadrupole component at the outskirts of the cluster is due to the anisotropy in the radiation field in the direction of the cluster center due to the SZE. Sunyaev and Zel'dovich discussed polarization due to the motion of the cluster with respect to the CMB and transverse to our line of sight (Sunyaev & Zel'dovich 1980b, see also Sazonov & Sunyaev 1999). In this case, the quadrupole comes from the Doppler shift. They found the largest terms to be of order $0.1\tau_e(v_{pec}/c)^2$ and $0.025\tau_e^2(v_{pec}/c)$ of the CMB intensity. The latter term, second order in τ_e , can be thought of as imperfect cancellation of the dipole term due to the anisotropic optical depth. Using $\tau_e = 0.01$ and a bulk motion of 500 km s⁻¹, results in polarization levels of order 10 nK, far beyond the sensitivity of current instrumentation.

The CMB as seen by the cluster electrons will have a quadrupole component and therefore the electron scattering will lead to linear polarization. This mechanism could possibly be used to trace the evolution of the CMB quadrupole if polarization measurements could be obtained for a large number of clusters binned in direction and redshift (Kamionkowski & Loeb 1997; Sazonov & Sun-

yaev 1999). Sazonov and Sunyaev calculated the expected polarization level and found the maximum CMB quadrupole induced polarization is $50(\tau_e/0.01)$ nK, somewhat higher than the expected velocity induced terms discussed above. The effect is again too small to expect detection in the near future. However, by averaging over many clusters, detecting this polarization might be possible with future satellite missions.

3 STATUS OF OBSERVATIONS

In the twenty years following the first papers by Sunyaev and Zel'dovich (Sunyaev & Zel'dovich 1970, 1972) there were few firm detections of the SZE despite a considerable amount of effort (Birkinshaw 1991). Over the last several years, however, observations of the effect have progressed from low S/N detections and upper limits to high confidence detections and detailed images. In this section we briefly review the current state of SZE observations.

The dramatic increase in the quality of the observations is due to improvements both in low-noise detection systems and in observing techniques, usually using specialized instrumentation to control carefully the systematics that often prevent one from obtaining the required sensitivity. The sensitivity of a low-noise radio receiver available 20 years ago should have easily allowed the detection of the SZE toward a massive cluster. Most attempts, however, failed due to uncontrolled systematics. Now that the sensitivities of detector systems have improved by factors of 3 to 10, it is clear that the goal of all modern SZE instruments is the control of systematics. Such systematics include, for example, the spatial and temporal variations in the emission from the atmosphere and the surrounding ground, as well as gain instabilities inherent to the detector system used.

The observations must be conducted on the appropriate angular scales. Galaxy clusters have a characteristic scale size of order a megaparsec. For a reasonable cosmology, a megaparsec subtends an arcminute or more at any redshift; low redshift clusters will subtend a much larger angle, for example the angular extent of the Coma cluster ($z = 0.024$) is of order a degree (core radius $\sim 10'$) (Herbig et al 1995). The detection of extended low surface brightness objects requires precise differential measurements made toward widely separated directions on the sky. The large angular scale presents challenges to control offsets due to differential ground pick-up and atmospheric variations.

3.1 Sources of Astronomical Contamination and Confusion

In designing an instrument for SZE observation, one also needs to take into account several sources of possible contamination and confusion from astronomical sources. One such source is anisotropy of the CMB itself (see Figure 3). For distant clusters with angular extents of a few arcminutes or less it is not a serious

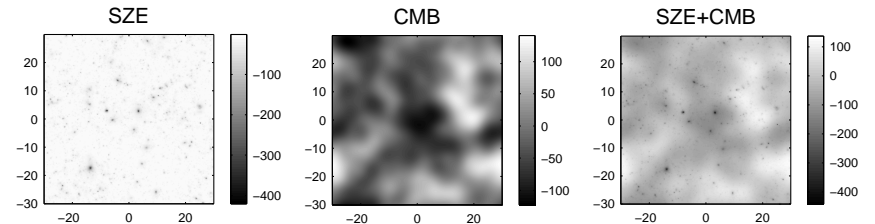


Figure 3: Illustration of the characteristic angular scales of primary CMB anisotropy and of the SZE. The images each cover one square degree and the gray scales are in μK . The left panel shows a image of the SZE from many clusters at 150 GHz (2 mm) obtained from a state-of-the-art hydrodynamic simulation (Springel et al 2001). The clusters appear point-like at this angular scale. The center panel is a realization of CMB anisotropy for a ΛCDM cosmology. The right panel illustrates that the SZE can be distinguished readily from primary CMB anisotropy provided the observations have sufficient angular resolution.

problem as the CMB anisotropy is expected (Hu & White 1997) and indeed found to be damped considerably on these scales (Church et al 1997; Subrahmanyan et al 2000; Dawson et al 2001, see also Holzapfel et al 1997 and LaRoque et al 2002 for CMB limits to SZE contamination). For nearby clusters, or for searches for distant clusters using beams larger than a few arcminutes, the intrinsic CMB anisotropy must be considered. The unique spectral behavior of the thermal SZE can be used to separate it from the intrinsic CMB in these cases. Note, however, that for such cases it will not be possible to separate the kinetic SZE effects from the intrinsic CMB anisotropy without relying on the very small spectral distortions of the kinetic SZE due to relativistic effects.

Historically, the major source of contamination in the measurement of the SZE has been radio point sources. It is obvious that emission from point sources located along the line of the sight to the cluster could fill in the SZE decrement, leading to an underestimate. The radio point sources are variable and therefore must be monitored. Radio emission from the cluster member galaxies, from the central cD galaxy in particular, is often the largest source of radio point source contamination, at least at high radio frequencies (Cooray et al 1998; LaRoque et al 2002). The typical spectral index of the radio point sources is $\alpha \sim 0.7$ for $S_\nu \propto \nu^{-\alpha}$, where S_ν is the point source flux. In the RJ limit, the SZE flux is proportional to ν^2 and therefore point sources are much less of an issue at higher radio frequencies.

Although it is most likely that insufficient attention to radio point sources would lead to the underestimate of the SZE effect, it could also lead to an overestimate. The most obvious example is if unaccounted point sources are in the

reference fields surrounding the cluster. An effect due to gravitational lensing has also been pointed out for low frequency observations where the flux from many point sources must be taken into account before a reliable measure of the SZE can be made. Essentially, gravitational lensing increases the efficiency of detecting point sources toward the center of the cluster which could lead to an overestimate of the SZE decrement (Loeb & Refregier 1997). This effect should be negligible at frequencies greater than roughly 30 GHz.

At frequencies near the null of the thermal SZE and higher, dust emission from extragalactic sources as well as dust emission from our own galaxy must be considered. Dust emission from our Galaxy rises steeply as $\nu^{2+\beta}$ with the observed dust opacity index β found to be $0 < \beta < 2$ over the frequencies of interest.

At the angular scales and frequencies of interest for most SZE observations, contamination from diffuse Galactic dust emission will not usually be significant and is easily compensated. Consider instead the dusty extragalactic sources such as those that have been found toward massive galaxy clusters with the SCUBA bolometer array (Smail et al 1997). Spectral indices for these sources are estimated to be $\sim 1.5-2.5$ (Blain 1998; Fischer & Lange 1993). Sources with 350 GHz (850 μm) fluxes greater than 8 mJy are common and all clusters surveyed had multiple sources with fluxes greater than 5 mJy. A 10 mJy source at 350 GHz corresponds to $\Delta T_{CMB} = 345 \mu K$ for 1' beam, or a Compton y -parameter of 6×10^{-5} . The same source scaled to 270 GHz, assuming a ν^2 spectrum, corresponds to $\Delta T_{CMB} = 140 \mu K$ at 270 GHz for 1' beam and a y -parameter of 6×10^{-5} . Scaling to the SZE thermal null at 218 GHz gives 3.9 mJy which corresponds to a $\Delta T_{CMB} = 85 \mu K$ for a 1' beam. This in turn translates directly to an uncertainty in a measurement of the cluster peculiar velocity (Eq. 6); for a massive cluster with an optical depth of 0.01 and an electron temperature of 10 keV, 85 μK corresponds to a peculiar velocity of 930 km s $^{-1}$. The contamination is more severe for less massive clusters with the dependence scaling as $\Delta v_{pec} \propto \tau_e^{-1} \propto R^2/M \propto M^{-1/3} \propto T_e^{-1/2}$. The contamination scales inversely with the beam area.

As with SZE observations at radio frequencies, the analyses of high frequency observations also need to consider the effects of point sources and require either high dynamic angular range, large spectral coverage, or both, to separate the point source emission from the SZE.

3.2 Single Dish Observations

All observations sensitive enough to observe the SZE are differential. The primary issue for single dish observations is how to switch the beam on the sky without introducing systematics comparable to the SZE. This beam switching can be accomplished in several ways, including but not limited to Dicke switch-

ing between feeds and chopping mirrors which switch or sweep the beam on the sky. With a single dish telescope, modulation of the beam sidelobes can lead to an offset. This offset can be removed if it remains stable enough to be measured on some portion of the sky without a cluster. However, temperature variations of the optics and features on the ground will cause the offset to change as the source is tracked. Therefore, it has become common practice to observe leading and trailing fields when they have the same position with respect to the ground as the source. In this way, any constant or linear drift in offset can be removed at the price of observing efficiency and sensitivity.

The first measurements of the SZE were made with single dish radio telescopes at centimeter wavelengths. Advances in detector technology made the measurements possible, although early observations appear to have been plagued by systematic errors that led to irreproducible and inconsistent results. Eventually, successful detections using beam switching techniques were obtained. During this period, the pioneering work of Birkinshaw and collaborators with the OVRO 40 meter telescope stands out for its production of results which served to build confidence in the technique (Birkinshaw et al 1978a,b; Birkinshaw 1991). More recently, leading and trailing beam switching techniques have been used successfully with the OVRO 5 meter telescope at 32 GHz to produce reliable detections of the SZE in several intermediate redshift clusters (Herbig et al 1995; Myers et al 1997; Mason et al 2001). The SEST 15 meter and IRAM 30 meter telescopes have been used with bolometric detectors at 140 GHz and chopping mirrors to make significant detections of the SZE effect in several clusters (Andreani et al 1996, 1999; Desert et al 1998; Pointecouteau et al 1999, 2001). The Nobeyama 45 m telescope has also been used at 21 GHz, 43 GHz, and 150 GHz to detect and map the SZE (Komatsu et al 2001, 1999).

In the Sunyaev-Zel'dovich Infrared Experiment (SuZIE), pixels in a six element 140 GHz bolometer array are electronically differenced by reading them out in a differential bridge circuit (Holzapfel et al 1997). Differencing in this way makes the experiment insensitive to temperature and amplifier gain fluctuations that produce 1/f noise. This increased low frequency stability allows SuZIE to observe in a drift scanning mode where the telescope is fixed and the rotation of the earth moves the beams across the sky. Using this drift scanning technique, the SuZIE experiment has produced high signal to noise strip maps of the SZE emission in several clusters (Holzapfel et al 1997; Mausekopf et al 2000a).

Because of the high sensitivity of bolometric detectors at millimeter wavelengths, single dish experiments are ideally suited for the measurement of the SZE spectrum. By observing at several millimeter frequencies these instruments should be able to separate the thermal and kinetic SZE's from atmospheric fluctuations and sources of astrophysical confusion. One of the first steps to realizing this goal is the measurement of SZE as an increment. So far, there have been only a few low signal to noise detections at a frequency of approximately 270

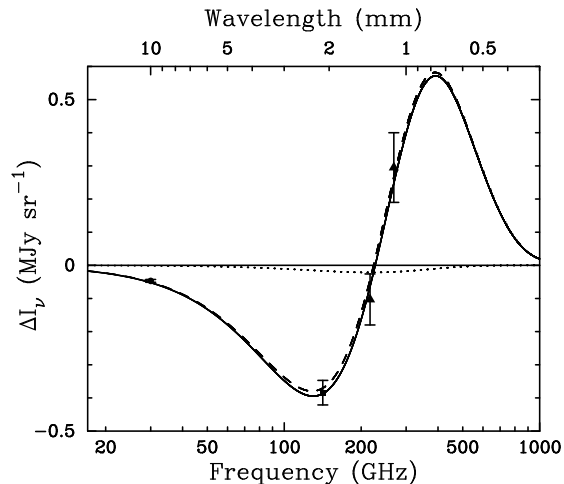


Figure 4: The measured SZE spectrum of Abell 2163. The data point at 30 GHz is from the Berkeley-Illinois-Maryland-Association (BIMA) array (LaRoque et al 2002), at 140 GHz it is the weighted average of Diabolo and SuZIE measurements (Desert et al 1998; Holzapfel et al 1997) and at 218 GHz and 270 GHz from SuZIE (Holzapfel et al 1997). The best fit thermal and kinetic SZE spectra are shown by the dashed line and the dotted lines, respectively, with the spectra of the combined effect shown by the solid line. The limits on the Compton y -parameter and the peculiar velocity are $y_0 = 3.56^{+0.41}_{-0.41} {}^{+0.27}_{-0.19} \times 10^{-4}$ and $v_p = 410^{+1030}_{-850} {}^{-460}_{-440}$ km s $^{-1}$, respectively, with statistical followed by systematic uncertainties at 68% confidence (Holzapfel et al 1997; LaRoque et al 2002).

GHz. The main reason for the lack of detection is the increased opacity of the atmosphere at higher frequencies. Holzapfel et al (1997) report a detection of Abell 2163 with the SuZIE instrument at 270 GHz. Andreani et al (1996) claim detections of the SZE increment in two clusters, although observations of a third cluster appear to be contaminated by foreground sources or systematic errors (Andreani et al 1999).

Figure 4 shows the measured SZE spectrum of Abell 2163, spanning the decrement and increment with data obtained from different telescopes and techniques (Holzapfel et al 1997; Desert et al 1998; LaRoque et al 2002). The SZE spectrum is a good fit to the data demonstrating the consistency and robustness of modern SZE measurements.

Single dish observations of the SZE are just beginning to reach their potential and the future is very promising. The development of large format millimeter

wavelength bolometer arrays will increase the mapping speed of current SZE experiments by orders of magnitude. The first of this new generation of instruments is the BOLOCAM 151 element bolometer array (Mauskopf et al 2000b; Glenn et al 1998) which will soon begin routine observations at the Caltech Submillimeter Observatory. BOLOCAM will observe in drift scanning mode and produce differences between bolometer signals in software. To the extent that atmospheric fluctuations are common across a bolometric array, it will be possible to realize the intrinsic sensitivity of the detectors. Operating from high astronomical sites with stable atmospheres and exceptionally low precipitable water vapor, future large format bolometer arrays have the potential to produce high signal to noise SZE images and search for distant SZE clusters with unprecedented speed.

3.3 Interferometric Observations

The stability and spatial filtering inherent to interferometry has been exploited to make high quality images of the SZE. The stability of an interferometer is due to its ability to perform simultaneous differential sky measurements over well defined spatial frequencies.

An interferometer measures the time averaged correlation of the signals received by a pair of telescopes – all interferometric arrays can be thought of as a collection of $n(n-1)/2$ two-element interferometers. For each pair of telescopes, the interferometer effectively multiplies the sky brightness at the observing frequency by a cosine, integrates the product and outputs the time average amplitude of the product (see Thompson et al 2001). In practice the signals are split and two correlations are performed with one being performed with a 90 degree relative phase shift so that the output of the interferometer, referred to as the visibility, is the complex Fourier transform (amplitude and phase) of the sky brightness. The interferometer is therefore only sensitive to angular scales (spatial frequencies) near B/λ , where the baseline B is the projected separation of the telescopes as seen by the source and λ is the observation wavelength. The interferometer response is essentially insensitive to gradients in the atmospheric emission or other large scale emission features.

There are several other features which allow an interferometer to achieve extremely low systematics. For example, only signals which correlate between array elements will lead to detected signal. For most interferometers, this means that the bulk of the sky noise for each element will not lead to signal. Amplifier gain instabilities for an interferometer will not lead to large offsets or false detections, although if severe they may lead to somewhat noisy signal amplitude. To remove the effects of offsets or drifts in the electronics as well as the correlation of spurious (non-celestial) sources of noise, the phase of the signal received at each telescope is modulated and then the proper demodulation is applied to the output of the correlator.

The spatial filtering of an interferometer also allows the emission from radio point sources to be separated from the SZE emission. This is possible because at high angular resolution ($\lesssim 10''$) the SZE contributes very little flux. This allows one to use long baselines – which give high angular resolution – to detect and monitor the flux of radio point sources while using short baselines to measure the SZE. Nearly simultaneous monitoring of the point sources is important as they are often time variable. The signal from the point sources is then easily removed, to the limit of the dynamic range of the instrument, from the short baseline data which are sensitive also to the SZE.

Figure 5 illustrates the spatial filtering of an interferometer with data on the galaxy cluster RXJ 1347 – 1145 from the BIMA interferometer outfitted with 30 GHz receivers (e.g., Carlstrom et al 1996; Carlstrom et al 2000). Panel *a*) shows the point source subtracted SZE image (contours) overlaid on a ROSAT X-ray image (color scale). Spatial scales typical of galaxy clusters were stressed before deconvolution. A higher resolution SZE image is shown in panel *b*), showing the range of spatial scales measured by the interferometer. Panel *c*) shows the long baseline (high angular resolution) data only. The bright on-center point source is readily apparent.

For the reasons given above, interferometers offer an ideal way to achieve high brightness sensitivity for extended low-surface brightness emission, at least at radio wavelengths. Most interferometers, however, were not designed for imaging low-surface brightness sources. Interferometers have been built traditionally to obtain high angular resolution and thus have employed large individual elements for maximum sensitivity to small scale emission. As a result special purpose interferometric systems have been built for imaging the SZE (Jones et al 1993; Carlstrom et al 1996; Padin et al 2000). All of them have taken advantage of low-noise high-electron-mobility-transistor (HEMT) amplifiers (Pospieszalski et al 1995) to achieve high sensitivity.

The first interferometric detection (Jones et al 1993) of the SZE was obtained with the Ryle Telescope (RT). The RT was built from the 5 Kilometer Array, consisting of eight 13 m telescopes located in Cambridge, England operating at 15 GHz with East-West configurations. Five of the telescopes can be used in a compact E-W configuration for imaging of the SZE (Jones et al 1993; Grainge et al 1993, 1996, 2000; Saunders et al 2000; Grainger et al 2001; Grainge et al 2001; Jones et al 2001).

The OVRO and BIMA SZE imaging project uses 30 GHz (1 cm) low noise receivers mounted on the OVRO¹ and BIMA² mm-wave arrays in California. They have produced SZE images toward 60 clusters to date (Carlstrom et al 1996, 2000; Patel et al 2000; Grego et al 2000; Reese et al 2000; Grego et al 2001; Joy

¹An array of six 10.4 m telescopes located in the Owens Valley, CA and operated by Caltech

²An array of ten 6.1 m mm-wave telescopes located at Hat Creek, California and operated by the Berkeley-Illinois-Maryland-Association

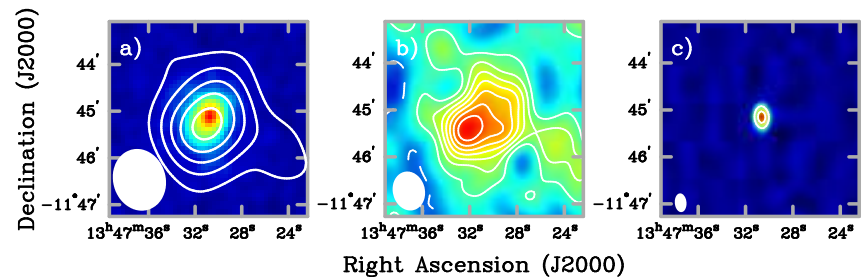


Figure 5: Interferometric images of the SZE of galaxy cluster RXJ 1347-1145 emphasizing different spatial scales. The FWHM ellipse of the synthesized beam is shown in the lower left corner of each panel. (a) Point source subtracted SZE image (contours) overlaid on ROSAT X-ray image (false color). The contours are multiples of $185\mu\text{K}$ ($\sim 2\sigma$), and negative contours are shown as solid lines. A 1500λ half-power radius Gaussian taper was applied to the u, v data resulting in a $63'' \times 80''$ synthesized beam. The X-ray image is HRI raw counts smoothed with a Gaussian with $\sigma = 6''$ and contains roughly 4000 cluster counts. (b) Higher resolution point source subtracted SZE image (both contours and false color). A 3000λ half-power radius Gaussian taper was applied resulting in a $40'' \times 50''$ synthesized beam. The contours are multiples of $175\mu\text{K}$ ($\sim 1\sigma$) (c) Image of the point source made using projected baselines greater than 3000λ . This map has a synthesized beam of $15'' \times 24''$ and a rms of $\sim 275\mu\text{Jy beam}^{-1}$, corresponding to a $\sim 1200\mu\text{K}$ brightness sensitivity. The contours are multiples of 15σ . The data was taken with the BIMA mm-array operating at 28.5 GHz. Single dish maps of the SZE toward RXJ 1347-1145 have also been made with the IRAM 30-m and the Nobeyama 45-m telescopes (Pointecouteau et al 2001; Komatsu et al 2001).

et al 2001; LaRoque et al 2002; Reese et al 2002). A sample of their SZE images is shown in Figure 6. Figure 6 also clearly demonstrates the independence of the SZE on redshift. All of the clusters shown have similar high X-ray luminosities and, as can be seen, the strength of the SZE signals are similar despite the factor of five in redshift. The OVRO and BIMA arrays support two dimensional configuration of the telescopes, including extremely short baselines, allowing good synthesized beams for imaging the SZE of clusters at declinations greater than ~ -15 degrees.

The Ryle Telescope, OVRO, and BIMA SZE observations are insensitive to the angular scales required to image low redshift clusters, $z \ll 0.1$. Recently, however, the Cosmic Background Imager (CBI) (Padin et al 2000) has been used to image the SZE in a few nearby clusters (Udomprasert et al 2000). The CBI is composed of thirteen 0.9 m telescopes mounted on a common platform with

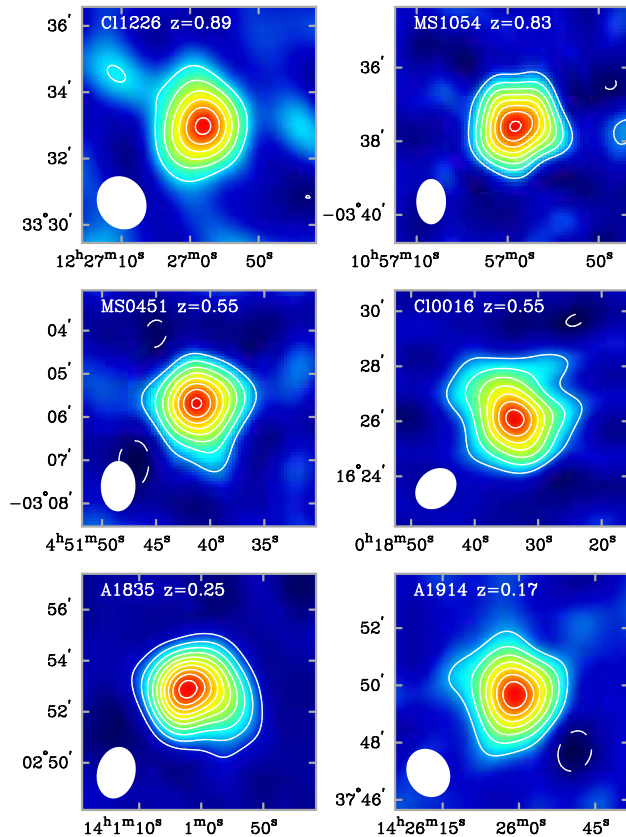


Figure 6: Deconvolved interferometric SZE images for a sample of galaxy clusters over a large redshift range ($0.17 \leq z \leq 0.89$). The contours are multiples of 2σ and negative contours are shown as solid lines. The FWHM ellipse of the synthesized beam is shown in the lower left corner of each panel. The noise level σ ranges from $25\mu\text{K}$ to $70\mu\text{K}$ for the clusters shown. Radio point sources were removed from a large fraction of the images shown. The interferometer was able to separate the point source emission from the SZE by using the high resolution data obtained with long baselines. All of the clusters shown have similar high X-ray luminosities and, as can be seen, the strength of the SZE signals are similar despite the factor of five in redshift, illustrating the independence of the SZE on redshift.

baselines spanning 1 m to 6 m. Operating in ten 1 GHz channels spanning 26 - 36 GHz, it is sensitive to angular scales spanning $3'$ to $20'$. The large field of view of the CBI, 0.75 degrees FWHM, makes it susceptible to correlated contamination from terrestrial sources, i.e., ground emission. To compensate, they have adopted the same observing strategy as for single dish observations (§3.2), and subtract data from leading and trailing fields offset by ± 12.5 minutes in Right Ascension from the cluster.

Interferometric observations of the SZE, as for single dish observations, are just beginning to demonstrate their potential. Upcoming instruments will be over an order of magnitude more sensitive. The OVRO - BIMA SZE imaging team is now building the Sunyaev-Zel'dovich Array (SZA), consisting of eight 3.5 m telescopes outfitted with 26 - 36 GHz and 85 - 115 GHz low-noise receivers and employing an 8 GHz wideband correlator. The SZA is expected to be operational by the end of 2003. It will be deployed with the existing six 10.4 m OVRO telescopes and nine 6.1 BIMA telescopes at a new high site if the site is ready in time. If not, the array will be deployed in the Owens Valley with the existing OVRO telescopes. The SZA will operate both in a dedicated survey mode and also as a fully heterogeneous array with the larger telescopes. The heterogeneous array will provide unprecedented imaging of the SZE at high resolution.

The Ryle Telescope (RT) SZE team is also building the ArcMinute Imager (AMI), consisting of ten 3.7m telescopes operating at 15 GHz near the RT in Cambridge. It is not planned to operate AMI as a heterogeneous array with the Ryle telescope, but the RT would be used for concurrent point source monitoring.

Additionally, plans have been discussed to reconfigure the CBI to 90 GHz. With its thirteen 0.9 m telescopes and 10 GHz bandwidth, the CBI would be a formidable SZE survey machine. A similar fixed platform interferometer, the Array for Microwave Background Anisotropy (AMiBA), is also being built with nineteen 1.2 m telescopes and operating at 90 GHz. AMiBA, like the reconfigured CBI, would also be ideally suited for performing SZE surveys at moderate resolution.

This next generation of interferometric SZE instruments will conduct deep SZE surveys covering tens and possibly hundreds of square degrees. While not as fast as planned large format bolometric arrays, the interferometers will be able to provide more detailed imaging. In particular, the high resolution and deep imaging provided by the SZA/OVRO/BIMA heterogeneous array (referred to as CARMA, the Combined ARray for Millimeter Astronomy) operating at 90 GHz will provide a valuable tool for investigating cluster structure and its evolution. As discussed in §5.5, such studies are necessary before the full potential of large SZE surveys for cosmology can be realized.

4 SKY SURVEYS WITH THE SZE

With recent developments in instrumentation and observing strategies, it will soon be possible to image large areas with high sensitivity, enabling efficient and systematic SZE searches for galaxy clusters.

The primary motivation for large surveys for galaxy clusters using the SZE is to obtain a cluster catalog with a well understood selection function that is a very mild function of cosmology and redshift. There are two primary uses for such a catalog. The first is to use clusters as tracers of structure formation, allowing a detailed study of the growth of structure from $z \sim 2$ or 3 to the present day. The second use is for providing a well-understood sample for studies of individual galaxy clusters, either as probes of cosmology or for studies of the physics of galaxy clusters.

Numerous authors have presented estimates of the expected yields from SZE surveys (Korolev et al 1986; Bond & Myers 1991; Bartlett & Silk 1994; Markevitch et al 1994; De Luca et al 1995; Bond & Myers 1996; Barbosa et al 1996; Colafrancesco et al 1997; Aghanim et al 1997; Kitayama et al 1998; Holder et al 2000b; Bartlett 2000; Kneissl et al 2001). Results from the diverse approaches to calculating the cluster yields are in broad agreement.

4.1 Cluster Abundance

The number of clusters expected to be found in SZE surveys depends sensitively on the assumed cosmology and detector specifications. Estimates of the order of magnitude, however, should be robust and able to give a good indication of the expected scientific yields of surveys for galaxy clusters using the SZE.

In calculating the number of clusters expected in a given survey, three things are needed:

- 1) the volume per unit solid angle as a function of redshift,
- 2) the number density of clusters as a function of mass and redshift, and
- 3) an understanding of the expected mass range which should be observable with the particular SZE instrument and survey strategy.

The physical volume per unit redshift per unit solid angle is given by (Peebles 1994)

$$\frac{dV}{d\Omega dz} = D_A^2 c \frac{dt}{dz} \quad , \quad (7)$$

where $dt/dz = 1/[H(z)(1+z)]$ and $H(z)$ is the expansion rate of the universe. The comoving volume is simply the physical volume multiplied by $(1+z)^3$.

The number density of clusters as a function of mass and redshift can either be derived by applying the statistics of peaks in a Gaussian random field (Press & Schechter 1974; Bond et al 1991; Sheth et al 2001) to the initial density perturbations or taken from large cosmological N-body simulations (Jenkins et al

2001). The mass function is still not understood perfectly, with small but important differences between competing estimates, especially at the high mass end of the spectrum. Precise cosmological studies will require an improved understanding, but reasonably accurate results can be obtained with the ‘‘standard’’ Press-Schechter (Press & Schechter 1974) mass function, with the comoving number density between masses M and $M + dM$ given by

$$\frac{dn(M, z)}{dM} = -\sqrt{\frac{2}{\pi}} \frac{\bar{\rho}}{M^2} \frac{d \ln \sigma(M, z)}{d \ln M} \frac{\delta_c}{\sigma(M, z)} \exp \left[\frac{-\delta_c^2}{2\sigma(M, z)^2} \right] \quad . \quad (8)$$

In the above, $\bar{\rho}$ is the mean background density of the universe today, $\sigma^2(M, z)$ is the variance of the density field when smoothed on a mass scale M , and δ_c (typically ~ 1.69) is the critical overdensity for collapse in the spherical collapse model (Peebles 1980).

Smoothing the density field on a mass scale corresponds to finding the comoving volume that encloses a given mass for a region at the mean density of the universe and smoothing the density field over this volume. The variance $\sigma^2(M, z)$ is separable as $\sigma(M, z) \equiv \sigma(M)D(z)$, where $\sigma(M)$ is the variance in the initial density field and $D(z)$ is the linear growth function that indicates how the amplitude of the density field has grown with time. For a universe with $\Omega_M = 1$ this growth function is simply proportional to the scale factor.

For a universe composed only of matter and vacuum energy (either with or without spatial curvature), accurate fitting functions for the growth function can be found in Carroll et al (1992) or can be found as a straightforward one-dimensional numerical integral, using the solution found by Heath (1977). For a more exotic universe, for example one with dark energy not in the form of a cosmological constant, the growth function requires solution of a two dimensional ordinary differential equation.

The Press-Schechter formulation has the advantage of making it clear that the abundance of very massive objects is exponentially suppressed, showing that massive clusters are expected to be rare. The amount of suppression as a function of redshift is sensitive to the linear growth function $D(z)$, which is itself sensitive to cosmological parameters. Structure grows most efficiently when the universe has $\Omega_M \sim 1$, so the growth function as a function of z should give a good indication of the epoch when either curvature, vacuum energy or dark energy started to become dynamically important.

The exponential dependence of the cluster abundance makes SZE surveys a potentially powerful probe of cosmology. This is shown in Figure 7, where the relative importance of volume and number density can be seen. A difference in cosmology can cause a difference in volume of a few tens of percent, while the corresponding change in comoving number density is typically a factor of a few. This plot also shows the rapid decline in the number density of the cluster abundance with redshift and its steep dependence on mass, both of which are

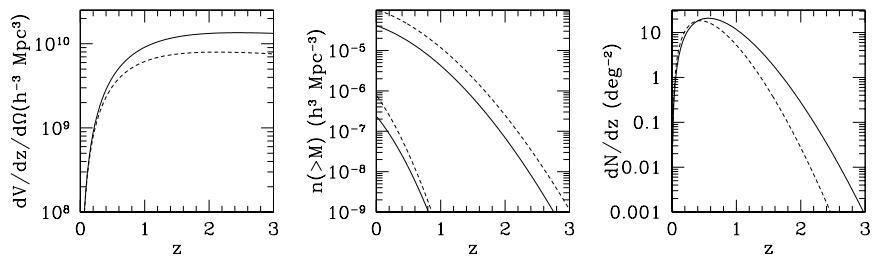


Figure 7: Comoving volume element (left) and comoving number density (center) for two cosmologies, $(\Omega_M, \Omega_\Lambda) = (0.3, 0.7)$ (solid) and $(0.5, 0.5)$ (dashed). For the middle panel, the normalization of the matter power spectrum was taken to be $\sigma_8 = 0.9$ and the Press-Schechter mass function was assumed. The lower set of lines in the middle panel correspond to clusters with mass greater than $10^{15} h^{-1} M_\odot$ while the upper lines correspond to clusters with mass greater than $10^{14} h^{-1} M_\odot$. The right panel corresponds to the cluster redshift distribution per square degree for clusters with masses greater than $10^{14} h^{-1} M_\odot$, with the normalization of the power spectrum adjusted ($\sigma_8 = 0.75$ for $\Omega_M = 0.5$) to produce the same local cluster abundance for both cosmologies. Note that in this case, fewer clusters are predicted at high redshift for the higher density cosmology.

due to the exponential suppression of high peaks.

The cosmology with the higher mass density can be seen to have a higher abundance at $z = 0$ in Figure 7 for a fixed normalization of the power spectrum, i.e., σ_8 . This is primarily because a given cluster mass will correspond to a slightly smaller size for a universe with higher matter density. The matter power spectrum rises toward smaller scales, so a fixed amplitude of the power spectrum on a specific scale will lead to a higher density cosmology having more power on a given mass scale. Choosing a slightly lower value of σ_8 for the cosmology with the higher density removes this offset in the cluster abundance at $z = 0$ and leads to a lower cluster abundance at higher redshifts, i.e., if the cluster abundance is normalized at $z = 0$ for all cosmological models, the higher density models will have relatively fewer clusters at high redshift. This can be seen in the right panel of Figure 7, where the redshift distribution per square degree has been normalized to give the same number of clusters above a mass of $10^{14} h^{-1} M_\odot$ at $z = 0$ by lowering the normalization of the power spectrum from $\sigma_8 = 0.90$ to 0.75 for the cosmology with the higher matter density.

4.2 Mass Limits of Observability

The range of masses to which a survey is sensitive is set by the effective beam size and sensitivity of the instrument as well as the cluster profile on the sky. In the case of a beam that is larger than the cluster, a survey is limited by SZE flux. From equation 5, a flux limit corresponds to constant $N_e T / D_\lambda^2$. The dependence on angular diameter distance rather than luminosity distance leads to a relative factor of $(1+z)^4$ when compared to a usual flux limit for emission from a distant source. Past $z \sim 1$ the angular diameter distance is slowly varying, and the gas temperature for a fixed mass should be higher than at $z = 0$, since the clusters are more dense and therefore more tightly bound, i.e., smaller. As a result, at $z > 1$ the limiting mass for an SZE survey is likely to be gently declining with redshift (Holder et al 2000b; Bartlett 2000; Kneissl et al 2001). Nearby clusters ($z < 0.2$) are likely to be at least partially resolved by most SZE surveys, making the mass selection function slightly more difficult to estimate robustly. It is not expected that the mass threshold of detectability should change more than a factor of $\sim 2 - 3$ for clusters with $z > 0.05$, making an SZE selected catalog remarkably uniform in redshift in terms of its mass selection function.

The expected cluster profiles are not well known, since there are very few known clusters at $z > 0.5$, and these are much more massive than the typical clusters expected to be found in deep SZE surveys. The total SZE flux from a cluster should be fairly robust against changes in cluster profiles due to substructure or merging. Broadly speaking, the SZE is providing an inventory of hot electrons. The characteristic temperature in a cluster is set by virial considerations, since the electrons are mainly heated by shocks due to infall. Kinetic energy of infalling gas should be converted into thermal energy in a time shorter than the Hubble time, suggesting that the thermal energy per particle must necessarily be on the order of GM/R . Therefore, it is very difficult to substantially alter the expected SZE flux for a cluster of a given mass.

The mass limit of detection corresponding to an SZE flux limited survey is shown in the left panel of Figure 8. The two types of surveys shown correspond to deep ground-based imaging of a few tens of square degrees down to μK sensitivities with arcminute resolution or wide-field surveys (similar to the *Planck Surveyor* satellite) with $\sim 5' - 10'$ resolution.

In contrast to the total integrated SZE flux, the concentration of SZE flux is very model dependent, with very compact clusters having high central decrements (or increments) but subtending a relatively small solid angle. The integrated SZE flux is thus a potentially very powerful criterion for controlling selection effects in samples for cluster studies. The clusters can first be found using integrated SZE flux and then investigated with high resolution SZE imaging.

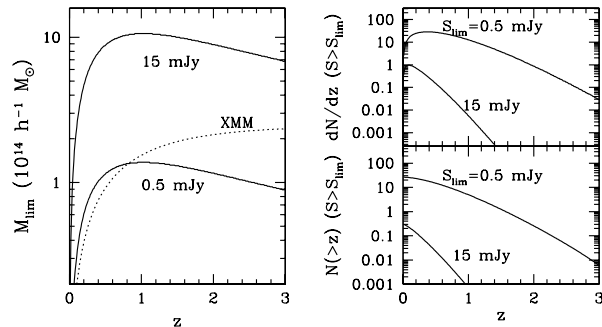


Figure 8: Left: Mass limits as a function of redshift for a typical wide-field type of survey (equivalent to ~ 15 mJy at 30 GHz) and a typical deep survey (~ 0.5 mJy). The approximate XMM serendipitous survey limit is also shown. Right: Differential (top) and cumulative (bottom) counts as a function of redshift for two SZE surveys shown at left, assuming a Λ CDM cosmology (Holder et al 2000b).

4.3 Estimates of SZE Source Counts

The expected source counts are shown in the right panels of Figure 8. From the considerations discussed above, it should be clear that the exact numbers will depend on cosmology and observing strategy. A robust conclusion is that upcoming deep surveys should find tens of clusters per square degree. Less deep surveys, such as the all-sky *Planck Surveyor* satellite survey should detect a cluster in every few square degrees. The resulting catalogs should be nearly uniformly selected in mass, with the deep catalogs extending past $z \sim 2$.

5 COSMOLOGY FROM SZE SURVEY SAMPLES

In this section we review the use of the SZE for cosmological studies and provide an update on current constraints. Emphasis is given to the cosmology that can, in principle, be extracted from SZE survey yields, as well as the observational and theoretical challenges which must be met before the full potential of SZE surveys for cosmology can be realized.

Future SZE surveys, with selection functions that are essentially a uniform mass limit with redshift (§4), will provide ideal cluster samples for pursuing cosmology. A large catalog of distant clusters will enable studies of large scale structure using the same methods as are applied to large catalogs of galaxies. The SZE surveys will also provide a direct view of the high redshift universe. Should clusters exist at redshifts much higher than currently predicted, i.e., if the initial mass fluctuations were non-Gaussian, they will be found by SZE surveys, but missed

in even the deepest X-ray observations planned.

The SZE survey samples can be used to increase the precision of the more traditional applications of the SZE to extract cosmological parameters, such as cluster distance measurements and the Hubble constant, the ratio Ω_B/Ω_M , and cluster peculiar velocities. These are discussed in §5.1, §5.2 and §5.3, respectively. The ability to derive these parameter depends primarily on the ability to use the SZE and other cluster observables to constrain or even overconstrain cluster properties. Precise SZE measurements will allow tests of the underlying assumptions in these derivations. For example, high resolution imaging of SZE, X-ray, and lensing, will allow detailed tests of the assumption of hydrostatic equilibrium (Miralda-Escude & Babul 1995; Loeb & Mao 1994; Wu & Fang 1997; Squires & Kaiser 1996; Allen & Fabian 1998). The sample yields will also allow the determination of global properties of clusters and their relationship to observables. For example, it is already possible to estimate cluster gas temperatures without X-ray data using current SZE data (Joy et al 2001).

The new frontier for SZE cosmology will be in exploiting the ability of future SZE surveys to measure cleanly the number density of clusters and its evolution in time. The redshift distribution of galaxy clusters is critically sensitive to Ω_M and the properties of the dark energy. For sufficiently large and deep SZE surveys, it is possible, in principle, to extract the equation of state of the dark energy. This is discussed in §5.4 and the theoretical and observational challenges are outlined in §5.5.

5.1 Distance Determinations, Hubble Constant

Several years after the SZE was first proposed (Sunyaev & Zel'dovich 1970, 1972) it was recognized that the distance to a cluster could be determined with a measure of its SZE and X-ray emission (Cavaliere et al 1977; Gunn 1978; Silk & White 1978; Cavaliere & Fusco-Femiano 1978; Birkinshaw 1979). The distance is determined by exploiting the different density dependencies of the SZE and X-ray emission. The SZE is proportional to the first power of the density; $\Delta T_{SZE} \sim \int dl n_e T_e$, where n_e is the electron density, T_e is the electron temperature, and dl is along the line-of-sight. The distance dependence is made explicit with the substitution $dl = D_A d\zeta$, where D_A is the angular diameter distance of the cluster.

The X-ray emission is proportional to the second power of the density; $S_x \sim \int dl n_e^2 \Lambda_{eH}$, where Λ_{eH} is the X-ray cooling function. The angular diameter distance is solved for by eliminating the electron density³ yielding

$$D_A \propto \frac{(\Delta T_0)^2 \Lambda_{eH0}}{S_{x0} T_{e0}^2} \frac{1}{\theta_c}, \quad (9)$$

where these quantities have been evaluated along the line of sight through the

³Similarly, one could eliminate D_A in favor of the central density, n_{e0}

center of the cluster (subscript 0) and θ_c refers to a characteristic scale of the cluster along the line of sight, whose exact meaning depends on the density model adopted. Only the characteristic scale of the cluster in the plane of the sky is measured, so one must relate the line of sight and plane of sky characteristic scales. For detailed treatments of this calculation see Birkinshaw & Hughes (1994) and Reese et al (2000). Combined with the redshift of the cluster and the geometry of the universe, one may determine the Hubble parameter, with the inverse dependencies on the observables as that of D_A . With a sample of galaxy clusters, one fits the cluster distances versus redshift to the theoretical angular diameter distance relation, with the Hubble constant as the normalization, e.g., see Figure 9.

There are two explicit assumptions made in SZE and X-ray distance determinations. The first one, mentioned above, is that the characteristic scale of the cluster along the line of sight must be related (usually assumed equal) to the scale in the plane of the sky. Typically, spherical symmetry is assumed for the cluster geometry since for a large sample of clusters one would expect $\langle \theta_c / \theta_c^{sky} \rangle = 1$, at least in the absence of selection effects. This assumption is supported by simulations as well (Sulkanen 1999). The second assumption is that $\langle n_e^2 \rangle^{1/2}$ equals $\langle n_e \rangle$ along the line of sight, i.e., that the clumping factor

$$C \equiv \frac{\langle n_e^2 \rangle^{1/2}}{\langle n_e \rangle}, \quad (10)$$

equals unity. If significant substructure exists in galaxy clusters, the derived Hubble constant will be overestimated by a factor of C^2 .

To date, there are 38 distance determinations to 26 different galaxy clusters from analyses of SZE and X-ray observations. In Figure 9 we show all SZE determined distances from high signal-to-noise SZE experiments. The uncertainties shown are statistical at 68% confidence. There are currently three samples of clusters with SZE distances: 1) a sample of 7 nearby ($z < 0.1$) galaxy clusters observed with the OVRO 5m telescope (Myers et al 1997; Mason et al 2001); 2) a sample of 5 intermediate redshift ($0.14 < z < 0.3$) clusters from the Ryle telescope interferometer (Jones et al 2001); and 3) a sample of 18 clusters with $0.14 < z < 0.83$ from interferometric observations by the OVRO and BIMA SZE imaging project (Reese et al 2002). A fit to the ensemble of 38 SZE determined distances yields $H_0 = 60 \pm 3 \text{ km s}^{-1} \text{ Mpc}^{-1}$ for an $\Omega_M = 0.3, \Omega_\Lambda = 0.7$ cosmology, where only the statistical uncertainty is included (at 68% confidence). The systematic uncertainty, discussed below, is of order 30% and clearly dominates. Since many of the clusters are at high redshift, the best fit Hubble constant will depend on the cosmology adopted; the best fit Hubble constant shifts to $56 \text{ km s}^{-1} \text{ Mpc}^{-1}$ for an open $\Omega_M = 0.3$ universe and to $54 \text{ km s}^{-1} \text{ Mpc}^{-1}$ for a flat $\Omega_M = 1$ geometry.

The prospects for improving both the statistical and systematic uncertainties

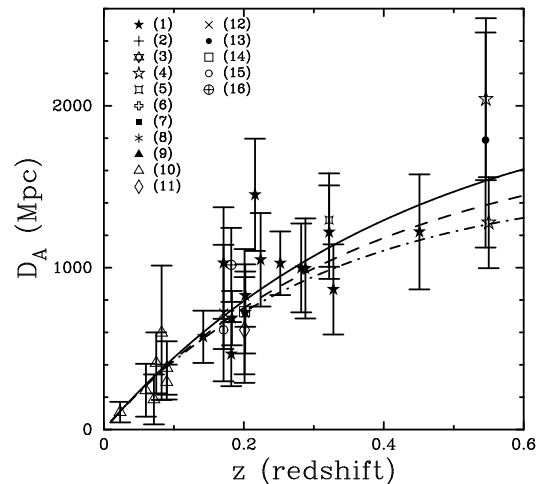


Figure 9: SZE determined distances versus redshift. The theoretical angular diameter distance relation is plotted for three different cosmologies, assuming $H_0 = 60 \text{ km s}^{-1} \text{ Mpc}^{-1}$: Λ $\Omega_M = 0.3, \Omega_\Lambda = 0.7$ (solid line); open $\Omega_M = 0.3$ (dashed); and flat $\Omega_M = 1$ (dot-dashed). The clusters are beginning to trace out the angular diameter distance relation. References: (1) Reese et al 2002; (2) Pointecouteau et al 2001; (3) Mauskopf et al 2000a; (4) Reese et al 2000; (5) Patel et al 2000; (6) Grainge et al 2000; (7) Saunders et al 2000; (8) Andreani et al 1999; (9) Komatsu et al 1999; (10) Mason et al 2001; Mason 1999; Myers et al 1997; (11) Lamarre et al 1998; (12) Tsuboi et al 1998; (13) Hughes & Birkinshaw 1998; (14) Holzapfel et al 1997; (15) Birkinshaw & Hughes 1994; (16) Birkinshaw et al 1991.

in the SZE distances in the near future are promising. Note, from Eq. 9, that the error budget in the distance determination is sensitive to the absolute calibration of the X-ray and SZE observations. Currently, the best absolute calibration of SZE observations is $\sim 2.5\%$ at 68% confidence based on observations of the brightness of the planets Mars and Jupiter. Efforts are now underway to reduce this uncertainty to the 1% level (2% in H_0). Uncertainty in the X-ray intensity scale also adds another shared systematic. The accuracy of the ROSAT X-ray intensity scale is debated, but a reasonable estimate is believed to be $\sim 10\%$. It is hoped that the calibration of the Chandra and XMM-Newton X-ray telescopes will greatly reduce this uncertainty.

The largest systematic uncertainties are due to departures from isothermality, the possibility of clumping, and possible point source contamination of the SZE

observations (for detailed discussion of systematics see, e.g., Birkinshaw 1999; Reese et al 2000, 2002). Chandra and XMM-Newton are already providing temperature profiles of galaxy clusters (e.g., Nevalainen et al 2000; Markevitch et al 2000; Tamura et al 2001). The unprecedented angular resolution of Chandra will provide insight into possible small scale structures in clusters. In addition, multi-wavelength studies by existing radio observatories, e.g., the Very Large Array (VLA), can shed light on the residual point source contamination of the radio wavelength SZE measurements. Therefore, though currently at the 30% level, many of the systematics can and will be addressed through both existing X-ray and radio observatories and larger samples of galaxy clusters provided from SZE surveys.

The beauty of the SZE and X-ray technique for measuring distances is that it is completely independent of other techniques, and that it can be used to measure distances at high redshifts directly. Since the method relies on the well understood physics of fully ionized plasmas, it should be largely independent of cluster evolution. Inspection of Figure 9 already provides confidence that a large survey of SZE distances consisting of perhaps a few hundred clusters with redshifts extending to one and beyond would allow the technique to be used to trace the expansion history of the universe, providing a valuable independent check of the recent determinations of the geometry of the universe from type Ia supernova (Riess et al 1998; Perlmutter et al 1999) and CMB primary anisotropy experiments (Pryke et al 2002; Netterfield et al 2002; Stompor et al 2001).

5.2 Cluster gas mass fractions, Ω_M

The ICM contains most of the baryons confined to the cluster potential with roughly an order of magnitude more baryonic mass than that observed in the galaxies themselves (White et al 1993; Forman & Jones 1982). The gas mass fraction, f_g , is therefore a reasonable estimate of the baryonic mass fraction of the cluster. It should also be reasonable approximation to the universal baryon mass fraction, $f_B \equiv \Omega_B/\Omega_M$, since it is not believed that mass segregation occurs on the large scales from which massive clusters condense ~ 1000 Mpc³. The cluster gas fraction is actually a lower limit, $f_g \leq f_B$, since a small fraction of baryons ($\sim 10\%$) are likely lost during the cluster formation process (White et al 1993; Evrard 1997), and we can not rule out the possibility of additional reservoirs of baryons in galaxy clusters which have yet to be detected.

A measurement of f_B leads directly to an estimate of Ω_M given a determination of Ω_B . Recent reanalysis of big bang nucleosynthesis predictions with careful uncertainty propagation (Burles et al 2001; Nollett & Burles 2000; Burles et al 1999) along with recent D/H measurements in Lyman α clouds (Burles & Tytler 1998; Burles & Tytler 1998) constrain the baryon density to be $\Omega_B h^2 = 0.020 \pm 0.002$ at 95% confidence. Recent CMB primary anisotropy experiments provide

an additional independent determination of $\Omega_B h^2$ consistent with the Lyman α cloud result (Pryke et al 2002; Netterfield et al 2002; Stompor et al 2001).

The gas mass is measured directly by observations of the SZE provided the electron temperature is known. The total gravitating mass can be determined by assuming hydrostatic equilibrium and using the distribution of the gas and, again, the electron temperature. The SZE derived gas fraction will therefore be proportional to $\Delta T_{SZE}/T_e^2$. Alternatively, the total gravitating mass can be determined by strong lensing (on small scales) or weak lensing (on large scales). Recently there has been considerable work on SZE gas fractions using total mass determinations derived under the assumption of hydrostatic equilibrium.

SZE derived cluster gas mass fractions have been determined for two samples of clusters and the results were used to place constraints on Ω_M : a sample of four nearby clusters (Myers et al 1997) and a sample of 18 distant clusters (Grego et al 2001). Both analyses used a spherical isothermal β -model for the ICM. The nearby sample was observed with the Owens Valley 5.5 m telescope at 32 GHz as part of a SZE study of an X-ray flux limited sample (Myers et al 1997). In this study, the integrated SZE was used to normalize a model for the gas density from published X-ray analyses, and then compared to the published total masses to determine the gas mass fraction. For three nearby clusters, A2142, A2256 and the Coma cluster, a gas mass fraction of $f_g h = 0.061 \pm 0.011$ at radii of 1-1.5 h^{-1} Mpc is found; for the cluster Abell 478, a gas mass fraction of $f_g h = 0.16 \pm 0.014$ is reported.

The high redshift sample of 18 clusters ($0.14 < z < 0.83$) was observed interferometrically at 30 GHz using the OVRO and BIMA SZE imaging system (Grego et al 2001). In this study, the model for the gas density was determined directly by the SZE data. X-ray emission weighted electron temperatures were used, but no X-ray imaging data was used. The gas fractions were computed from the data at a 1' radius where they are best constrained by the observations. Numerical simulations suggest, however, that the gas mass fraction at r_{500} (the radius inside of which the mean density of the cluster is 500 times the critical density) should reflect the universal baryon fraction (Evrard 1997; Evrard et al 1996; David et al 1995). The derived gas fractions were therefore extrapolated to r_{500} using scaling relations from cluster simulations (Evrard 1997). The resulting mean gas mass fractions are $f_g h = 0.081^{+0.009}_{-0.011}$ for $\Omega_M = 0.3$, $\Omega_\Lambda = 0.7$, $f_g h = 0.074^{+0.008}_{-0.009}$ for $\Omega_M = 0.3$, $\Omega_\Lambda = 0.0$ and $f_g h = 0.068^{+0.009}_{-0.008}$ for $\Omega_M = 1.0$, $\Omega_\Lambda = 0.0$. The uncertainties in the electron temperatures contribute the largest component to the error budget.

The angular diameter distance relation, $D_\Lambda(z)$, enters the gas fraction calculation and introduces a cosmology dependence on the results of the high z sample. In addition, the simulation scaling relations used to extrapolate the gas fractions to r_{500} have a mild dependence on cosmology. Figure 10 shows the constraints on Ω_M implied by the measured gas mass fractions assuming a flat universe

($\Omega_\Lambda \equiv 1 - \Omega_M$) and $h = 0.7$ to calculate D_A and the r_{500} scaling factor. The upper limit to Ω_M and its associated 68% confidence interval is shown as a function of Ω_M . The measured gas mass fractions are consistent with a flat universe and $h = 0.7$ when Ω_M is less than 0.40, at 68% confidence. For the measurements to be consistent with $\Omega_M = 1.0$ in a flat universe, the Hubble constant must be very low, h less than ~ 0.30 .

To estimate Ω_M , we need to account for the baryons contained in the galaxies and those lost during cluster formation. The galaxy contribution is assumed to be a fixed fraction of the cluster gas, with the fraction fixed at the value observed in the Coma cluster, $M_g^{true} = M_g^{obs}(1 + 0.20h^{3/2})$ (White et al 1993). Simulations suggest that the baryon fraction at r_{500} will be a modest underestimate of the true baryon fraction $f_g(r_{500}) = 0.9 \times f_B(\text{universal})$ (Evrard 1997). These assumptions lead to $f_B = [f_g(1 + 0.2h^{3/2})/0.9]$. Using this to scale the gas fractions derived from the high z SZE cluster sample and assuming $h = 0.7$ and a flat cosmology, leads to the constraints illustrated in Figure 10 with a best estimate $\Omega_M \sim 0.25$ (Grego et al 2001).

Cluster gas mass fractions can also be determined from cluster X-ray emission in a similar manner as from SZE measurements. However, there are important differences between X-ray and SZE determined gas fractions. For example, the X-ray emission is more susceptible to clumping of the gas, C , since it is proportional to the ICM density squared. On the other hand, the X-ray derived gas mass is essentially independent of temperature for the ROSAT 0.1-2.4 keV band used in the analyses (Mohr et al 1999), while the SZE derived gas mass is proportional to T_e^{-2} .

Currently X-ray data for low redshift clusters is of exceptional quality, far surpassing SZE data. X-ray based gas mass fractions have been measured to cluster radii of 1 Mpc or more (e.g., White & Fabian 1995; David et al 1995; Neumann & Bohringer 1997; Squires et al 1997; Mohr et al 1999). A mean gas mass fraction within r_{500} of $f_g h^{3/2} = 0.0749 \pm 0.0021$ at 90% confidence was derived from X-ray data from a large, homogeneous, nearby sample of clusters with $T_e > 5$ keV (Mohr et al 1999). The gas mass fractions derived from SZE measurements depend differently on the cosmology assumed than those derived from X-ray images, and this should be noted when comparing the results. Qualitatively, the comparison does not suggest any large systematic offsets. In fact, for a Λ CDM cosmology, solving for h from the combination of the Grego et al (2001) and Mohr et al (1999) results gives $h = 0.85_{-0.20}^{+0.30}$ at 68% confidence. This is significant, because a large clumping factor, $C \gg 1$ (see Eq. 10), has been suggested as an explanation for the high gas mass fractions in clusters (White et al 1993; Evrard 1997).

Cluster gas mass fractions can also be measured by comparing SZE derived gas masses and weak lensing derived total masses. The comparison is particularly interesting as both are measures of projected mass distributions. In addition, gas

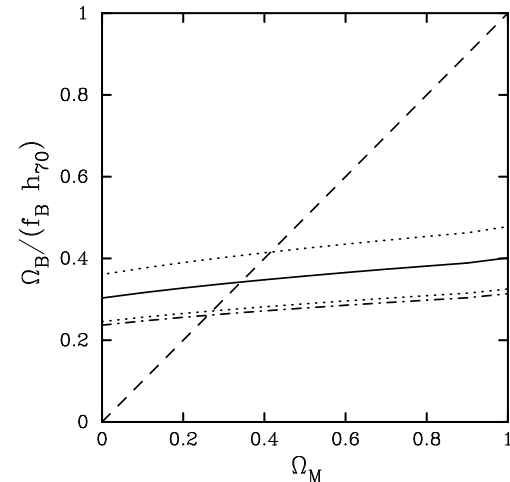


Figure 10: Limits on Ω_M from SZE measured cluster gas fractions (Grego et al 2001). Upper limit on the total matter density, $\Omega_M \leq \Omega_B/(f_B h_{70})$ (solid line) and its associated 68% confidence region (dotted lines), as a function of cosmology with $\Omega_\Lambda \equiv 1 - \Omega_M$. The intercept between the upper dotted line and the dashed line $\Omega_M = \Omega_B/(f_B h_{70})$ gives the upper limit to Ω_M at 68% confidence. The dot-dashed line shows the total matter density when the baryon fraction includes an estimate of the contribution from baryons in galaxies and those lost during cluster formation. The intercept of the dot-dashed line and the dashed line gives the best estimate of $\Omega_M \sim 0.25$ assuming a flat universe with $h = 0.7$.

mass fractions can be derived without assuming a model for the cluster structure and without assuming hydrostatic equilibrium. Comparisons of SZE and lensing data has only been done for a few clusters to date (Holder et al 2000a). However, as for the SZE, the quality and quantity of weak lensing observations toward galaxy clusters is rapidly increasing and several weak lensing surveys are underway. Holder et al (2000a) demonstrated that gas mass fractions can be determined from the analysis of SZE and weak lensing measurements without need to parameterize the ICM distribution. Furthermore, by comparing this mass fraction with one derived by assuming hydrostatic equilibrium, it is possible to solve for the ICM electron temperature and the angular diameter distance.

SZE surveys will provide a large catalog of galaxy clusters at redshifts $z > 1$. The increased sensitivity and larger angular dynamic range of the next generation of SZE instruments will allow measurements of cluster gas fractions to r_{500} directly, greatly increasing the precision of the gas mass fractions. Moreover,

extending the gas fraction analyses to high redshift will enable studies of the evolution of cluster structure. It should, for example, be straight forward to test speculative theories of dark matter decay (Cen 2001).

5.3 Cluster Peculiar Velocities

The kinetic SZE is a unique and potentially powerful cosmological tool as it provides the only known way to measure large scale velocity fields at high redshift (§2.2). To obtain an accurate measure of the peculiar velocity of a galaxy cluster, sensitive multifrequency SZE observations are required to separate the thermal and kinetic effects. From inspection of Figure 2, it is clear that measurements of the kinetic SZE are best done at frequencies near the null of the thermal effect at ~ 218 GHz. However, as discussed in §3.1, contamination by CMB temperature fluctuations as well as other sources make it difficult to determine accurately the peculiar velocity for a given cluster. There have been only a few recent attempts to measure the kinetic SZE.

The first interesting limits on the peculiar velocity of a galaxy cluster were reported in Holzapfel et al (1997). They used the Sunyaev-Zel'dovich Infrared Experiment (SuZIE) to observe Abell 2163 ($z = 0.202$) and Abell 1689 ($z = 0.183$) at 140 GHz (2.1 mm), 218 GHz (1.4 mm) and 270 GHz (1.1 mm). These observations include and bracket the null in the thermal SZE spectrum. Using a β model, with the shape parameters (θ_c , β) from X-ray data, they found $v_{pec} = +490_{-880}^{+1370}$ km s $^{-1}$ for Abell 2163 and $v_{pec} = +170_{-630}^{+815}$ km s $^{-1}$ for Abell 1689, where the uncertainties are at 68% confidence and include both statistical and systematic uncertainties. These results are limited by the sensitivity of the SZE observations, which were limited by differential atmospheric emission. The SuZIE data for Abell 2163 were reanalyzed with the addition of higher frequency measurements which are sensitive to emission from Galactic dust in the direction of the cluster (Lamarre et al 1998). More recently LaRoque et al (2002) also reanalyzed all of the available data for Abell 2163, including a new measurement obtained with the OVRO and BIMA SZE imaging system at 30 GHz (1 cm). As shown in Figure 4, the data is well fitted by parameters similar to the original values from Holzapfel et al (1997). The agreement between the measurements using different instruments and techniques is striking.

The intrinsic weakness of the kinetic SZE and the degeneracy of its spectrum with that of primary CMB fluctuations make it exceeding difficult to use it to measure the peculiar velocity of a single cluster. It may be possible, however, to determine mean peculiar velocities on extremely large scales by averaging over many clusters.

5.4 Energy Densities in the Universe and Growth of Structure

The evolution of the abundance of galaxy clusters is a sensitive probe of cosmology (§4). Measurements of the clusters masses and number density as a function of redshift can be used to constrain the matter density, Ω_M , and, for sufficiently large samples, the equation of state of the dark energy. X-ray surveys have already been used to constrain Ω_M (e.g., Borgani et al 2001; Viana & Liddle 1999; Bahcall & Fan 1998; Oukbir et al 1997), but they have been limited by sample size and their reduced sensitivity to high redshift clusters. SZE surveys offer the attractive feature of probing the cluster abundance at high redshift as easily as the local universe; as discussed in §4.2, the sensitivity of a SZE survey is essentially a mass limit (Bartlett & Silk 1994; Barbosa et al 1996; Holder et al 2000b; Bartlett 2000; Kneissl et al 2001).

The simple mass selection function of SZE surveys could allow the source count redshift distribution to be used as a powerful measure of cosmological parameters (Barbosa et al 1996; Haiman et al 2001; Holder et al 2001; Weller et al 2001; Benson et al 2001) and the structure formation paradigm in general. As an example, we show in Figure 11 the expected constraints in Ω_M - Ω_Λ - σ_8 parameter space from the analysis of a deep SZE survey (Carlstrom et al 2000; Holder et al 2000b; Holder et al 2001) covering 12 square degrees in which all clusters above $10^{14} h^{-1} M_\odot$ are detected and for which redshifts have been obtained. The darkest region corresponds to the 68% confidence region, red to 95%. The shaded regions show the result of a Monte Carlo method for estimating confidence regions. Many realizations of a fiducial model ($\Omega_M=0.3$, $\Omega_\Lambda=0.7$, $\sigma_8=1$) were generated and fit in the three-dimensional parameter space, and the shaded regions indicate regions which contain 68% and 95% of the resulting best fits. The contours show confidence regions from a Fisher matrix analysis, where the confidence regions are assumed to be Gaussian ellipsoids in the parameter space. In each case, the dimension not shown has been marginalized over, rather than kept fixed.

The next generation of dedicated telescopes equipped with large format bolometer detector arrays offers the possibility of conducting SZE surveys over thousands of square degrees with $\lesssim 10\mu K$ sensitivity. As shown in Figure 12, the yields from such a survey should, in principle (see §5.5), enable highly accurate estimation of cosmological parameters, notably of the matter density and the properties of the dark energy. Most importantly, the degeneracies in the constraints of the cosmological parameters derived from SZE survey yields are very different from those expected from distance measures or CMB measurements. This simply arises because clusters are probing a fundamentally different physical effect, the growth rate of structure, rather than distance. Both growth and distance are related to the expansion history of the universe, but the two measures are effectively sensitive to different moments of the expansion rate.

A generic prediction of inflation is that the primordial fluctuations should be Gaussian. With cluster surveys probing the highest peaks of the density field,

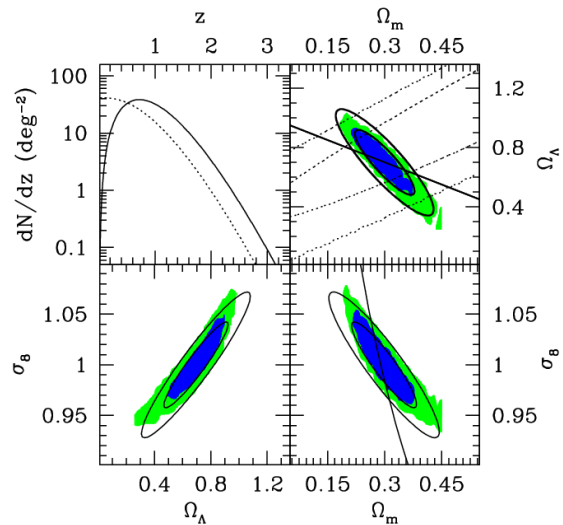


Figure 11: Expected constraints in the Ω_M - Ω_Λ (top right), Ω_M - σ_8 (bottom right), and Ω_Λ - σ_8 (bottom left) planes from the analysis of a SZE survey covering 12 square degrees in which all clusters above $10^{14}h^{-1} M_\odot$ are detected and the redshifts are known. The top left panel shows the expected redshift distribution of clusters (solid line) with the cumulative $N(> z)$ shown as a dotted line. In the other panels, the 68% confidence regions are shown by the darkest shaded regions, and the 95% confidence by the lighter regions. The solid contours correspond to the same confidence regions derived from an approximate method. In each panel the dimension not shown has been marginalized over rather than kept fixed. In the upper right panel, the broken line diagonal ellipses are the constraints based on the analyses of type Ia Supernova at 68% and 95% confidence (Riess et al 1998; Perlmutter et al 1999). The diagonal line at $\Omega_M + \Omega_\Lambda = 1$ is for a flat universe as suggested by recent CMB anisotropy measurements (Miller et al 1999; de Bernardis et al 2000; Hanany et al 2000; Pryke et al 2002). The solid line in lower right panel shows the approximate direction of current constraints (Viana & Liddle 1999).

non-Gaussianity in the form of an excess of high peaks should be readily apparent, especially at high redshift (Benson et al 2001). Cluster surveys are therefore probing both the structure formation history of the universe and the nature of the primordial fluctuations. In this way, cluster surveys are emerging as the next

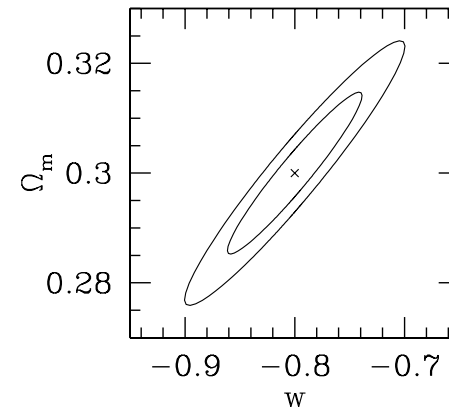


Figure 12: Expected constraints on the matter density Ω_M and the dark energy equation of state w from the analysis of a SZE survey covering several thousand square degrees in which all clusters above $2.5 \times 10^{14}h^{-1} M_\odot$ are detected and the redshifts are known. The normalization of the power spectrum has been marginalized over, and contours show 68% and 95% confidence regions for two parameters. Note, that no systematic errors have been assumed in deriving the cosmological constraints. As discussed in the text, considerable observational and theoretical work needs to be done before such tight constraints could be extracted from large scale SZE surveys.

serious test of the cold dark matter paradigm.

5.5 Challenges for Interpreting SZE Surveys

In order to realize the full potential of the evolution of the cluster number density as a cosmological probe, a strong understanding of the physics of galaxy clusters will be required. As fully collapsed objects, the complete physics of galaxy clusters is highly non-linear and complex. The size of such massive objects, however, makes them insensitive to disruption from most physical mechanisms. Nevertheless, there are several important aspects of gas dynamics that could affect interpretation of SZE galaxy cluster surveys.

The SZE is only sensitive to free electrons; any process that removes electrons from the optically thin ICM can affect the magnitude of the SZE for a given total mass. For example, cooling of the ICM, star formation or heating of the

ICM from supernovae can affect the observed SZE (Holder & Carlstrom 1999; Springel et al 2001; Holder & Carlstrom 2001; Benson et al 2001). If the cooling or star formation is not dependent on cluster mass or redshift, this can be simply calibrated and accounted for in deriving the survey selection function. The most promising theoretical path for understanding such processes is through high resolution cosmological simulations that include the relevant gas dynamics; such simulations are only now becoming feasible. The possible effects of such gas dynamics are shown in Figure 13 (Holder & Carlstrom 2001). A simple model has been adopted for this figure, where some combination of heating or cooling has reduced the number of hot electrons in the central regions of galaxy clusters by an amount that is modeled through the effects of an “entropy floor” (Ponman et al 1999). The curves in this figure show the extreme cases of either no heating or cooling (no entropy floor) or extreme gas evolution, with an assumed value for the minimum entropy that is roughly a factor of two larger than is required for consistency with the observations (Ponman et al 1999). Changing the evolution of the ICM could mimic changes in cosmological parameters at levels much larger than the expected statistical errors. With detailed imaging of the ICM using SZE and X-ray telescopes, the effects of heating or cooling should be apparent, so the possible systematic errors due to heating or cooling should in practice be much smaller than 10% in Ω_M .

Although the SZE-mass relation is easy to understand theoretically in general terms, the details of the normalization and redshift evolution will require additional studies of at least a moderately sized SZE cluster catalog. For example, simple scaling arguments can be used to estimate the expected relation between cluster mass and temperature, but the exact cosmological dependence could be sensitive to merger rates as a function of cosmology or other non-linear effects.

Furthermore, the mapping between the initial density field and the number density of clusters of a given mass as a function of redshift, i.e., the mass function, is not known perfectly at this time. The current generation of large cosmological simulations offers hope for a much better understanding in coming years. An important use for a large scale SZE cluster survey will be to characterize this mass function and test the reliability of various analytical (Press & Schechter 1974; Bond et al 1991; Sheth et al 2001) and numerical (Jenkins et al 2001) estimates.

In order to exploit fully the potential of SZE surveys, the limiting mass as a function of redshift for galaxy clusters will have to be understood to an accuracy of better than 5% and uncertainties in the mass function must be reduced to better than 10% (Holder et al 2001). The former will require a concerted observational effort and is likely to be the most difficult to achieve; the latter requirement is not far from current uncertainties (Jenkins et al 2001). Note that it is not required that we know the mass of each cluster in the catalog to this accuracy, but only that we can characterize the cluster detection efficiency as a function of mass to

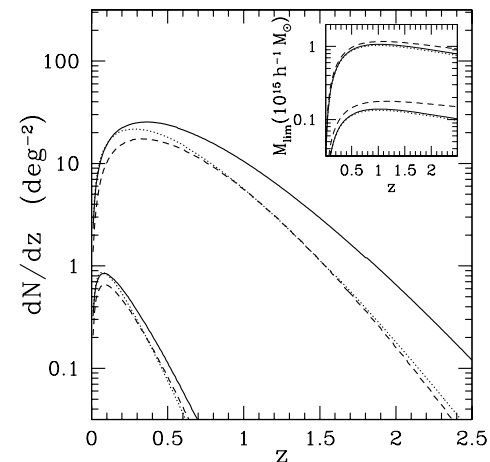


Figure 13: Effects of gas evolution on cluster survey yields. In the inset, the top group of lines correspond to mass limits for a SZE survey similar to the *Planck Surveyor* satellite survey, with the uppermost line indicating the expected mass limit for a model with significant gas heating while the lower line in the top group shows the expected mass limit of detection for the case of no cluster gas heating. The cosmology chosen is $\Omega_M=0.3, \Omega_\Lambda=0.7, \sigma_8 = 1$. The lower set of lines show the same effects for a deep SZE survey. The main panel shows the expected redshift distributions for the mass limits in the inset. In the main panel the top group of lines correspond to the deep surveys while the lower group correspond to *Planck Surveyor*. The solid line within each set shows the expected counts for the case of no heating, while the dashed line shows the effect of gas heating. The dotted curve, i.e., the middle curve in each set, shows a model with no heating but with $\Omega_M=0.33$ and σ_8 modified to keep the same number of clusters at $z = 0$ (Holder & Carlstrom 2001). The assumptions of no heating and the very high value of heating for this plot are extreme and should bracket the true gas evolution.

this level.

While some of the theory of the physics of galaxy clusters is not known, there are plenty of observational diagnostics which can be used in the interpretation of SZE surveys. High resolution SZE imaging of high redshift clusters will provide information on the relative importance of gas dynamics (Holder & Carlstrom 2001) to the observed properties of galaxy clusters. The main effect of most gas processes should be to cause the gas to be less centrally concentrated, either because the low-entropy gas has been removed (Bryan 2000) or because the gas

has gained entropy from non-gravitational heating.

It may also be possible with the next generation of large format multi-frequency bolometer arrays to exploit the small relativistic corrections to the SZE spectrum to determine the gas temperature. Such measurements will allow an understanding of temperature structure in the gas, even without follow-up X-ray observations. A direct SZE-weighted temperature would be more directly relevant to the SZE observations in determining the gas mass, and comparisons with X-ray spectral temperatures, when possible, could provide valuable information on the temperature structure along the line of sight. Temperature information, combined with high-resolution imaging, allows a reconstruction of the cluster potential and therefore can provide important constraints on the gas mass fraction as a function of radius as well as a diagnostic for the effects of gas cooling.

In terms of the properties of the cluster catalog produced by a SZE survey, it is difficult to avoid the conclusion that the survey limit will be mainly dependent only on cluster mass and that this mass limit will be relatively flat with redshift beyond $z \sim 0.1$. This will make the resulting catalog especially useful for studies of the physics of galaxy clusters. The requirements on understanding the cluster mass selection function for such studies are much less strict than those required for cosmological studies. The results from detailed studies of individual clusters in the catalog will naturally feed back and improve our understanding of the survey selection function.

6 SUMMARY

The SZE is emerging as a powerful tool for cosmology. Over the last several years, detection of the SZE toward massive galaxy clusters has become routine, as has high quality imaging at moderate angular resolution of order an arcminute. Measurements of the effect already have been used to place interesting constraints on the Hubble constant and, through measurements of cluster gas mass fractions, the matter density of the universe, Ω_M .

The next step is to exploit the redshift independence of the SZE signal to conduct blind surveys for galaxy clusters. The limit for such a survey is essentially a mass limit that is remarkably uniform with redshift. The cluster catalog from such a unbiased survey could be used to greatly increase the precision and redshift range of present SZE constraints on the Hubble constant and Ω_M , and could, for example, allow $D_A(z)$ to be determined to high redshift ($z \sim 2$).

The most powerful use of the SZE for cosmology will be the measurement of the evolution of the abundance of galaxy clusters. SZE surveys are ideally suited for this since they are able to probe the abundance at high redshift as easily as the local universe. The evolution of the abundance of galaxy clusters is a sensitive probe of cosmology. For example, the yields from a deep SZE survey covering only ten square degrees would be able to place interesting constraints on Ω_M ,

Ω_Λ , and σ_8 .

A generic prediction of inflation is that the primordial density fluctuations should be Gaussian. Non-Gaussianity in the form of an excess of high mass clusters should be readily apparent, especially at high redshift, from SZE survey yields. SZE cluster surveys will therefore probe both the structure formation history of the universe and the nature of the primordial fluctuations. In this way, cluster surveys are emerging as the next serious test of the cold dark matter paradigm.

Current SZE observations, while routine, require substantial integration time to secure a detection; a prohibitively long time would be required to conduct blind surveys over a large region of sky with the instruments now available. However, the next generation of instruments now being built or planned will be substantially faster. Dedicated interferometric arrays being built will be able to conduct deep SZE surveys over tens of square degrees. Heterogeneous arrays, such as the SZA combined with the OVRO array, will also allow detailed high resolution follow up SZE observations of the resulting cluster catalog.

A dedicated, low noise, single dish telescope with $\sim 1'$ resolution, equipped with a next generation, large format bolometric array receiver (~ 1000 elements) and operating from a superb site would be able to conduct a deep SZE survey over thousands of square degrees. The statistics provided by the yields from such a large survey ($\sim 10^4$ clusters) in the absence of systematic effects and assuming redshifts are known would be sufficient to determine precise constraints on Ω_M , Ω_Λ , σ_8 , and even set meaningful constraints on the equation of state of the dark energy.

The possible systematics that could affect the yields of SZE surveys are presently too large to realize the full potential of a deep SZE survey covering thousands of square degrees. The systematics include, for example, the uncertainties on the survey mass detection limit due to unknown cluster structure and cluster gas evolution, as well as the uncertainties in the theoretical mapping between the initial density field and the number density of clusters of a given mass as a function of redshift, i.e., the mass function.

These systematics can begin to be addressed through detailed follow-up observations of a moderate area SZE survey (tens of square degrees). High resolution SZE, X-ray, and weak lensing observations will provide insights into evolution and structure of the cluster gas. Numerical simulations directly compared and normalized to the SZE yields should provide the necessary improvement in our understanding of the mass function.

It is not unreasonable to consider the possibility of a space-based telescope operating at centimeter through submillimeter wavelengths with high angular resolution (< 1 arcminute) and good spectral coverage. For studies of the SZE, this would allow simultaneous determinations of electron column densities, temperatures, and peculiar velocities of galaxy clusters. Such a satellite would make

detailed images of the cosmic microwave background, while also providing important information on the high frequency behavior of radio point sources and the low frequency behavior of dusty extragalactic submillimeter sources. The upcoming *Planck Surveyor* satellite is a first step in this direction; it should provide an SZE all-sky survey although at moderate, ~ 5 arcminute, resolution. Such a survey should find on the order of $10^4 - 10^5$ clusters, most of them at redshift $z < 1$.

We can look forward to the SZE emerging further as a unique and powerful tool in cosmology over the next several years as the next generation of SZE instruments come online and SZE surveys become a reality.

ACKNOWLEDGEMENTS

We thank M. Joy and W. Holzapfel for their considerable input to this review and W. Hu, S. LaRoque, A. Miller, J. Mohr, and D. Nagai for their comments on the manuscript. We also thank M. White and C. Pryke for assistance with Figure 3. This work was supported in part by NASA LTSA account NAG5-7986 and NSF account AST-0096913. JEC also acknowledges support from the David and Lucile Packard Foundation and the McDonnell Foundation. EDR acknowledges support from a NASA GSRP fellowship (NGT5-50173) and a Chandra Fellowship (PF1-20020).

Literature Cited

Aghanim N, De Luca A, Bouchet FR, Gispert R, Puget JL. 1997. *A&A* 325:9–18
 Allen SW, Fabian AC. 1998. *MNRAS* 297:L57–L62
 Andreani P, Böhringer H, Dall’Oglio G, Martinis L, Shaver P, et al. 1999. *ApJ* 513:23–33
 Andreani P, Pizzo L, dall’Oglio G, Whyborn N, Böhringer H, et al. 1996. *ApJ* 459:L49–L52
 Bahcall N, Fan X. 1998. *ApJ* 504:1–6
 Barbosa D, Bartlett J, Blanchard A, Oukbir J. 1996. *A&A* 314:13–17
 Bartlett JG. 2000. *A&A* submitted: astro-ph/0001267
 Bartlett JG, Silk J. 1994. *ApJ* 423:12–18
 Benson AJ, Reichardt C, Kamionkowski M. 2001. *MNRAS* submitted:astro-ph/0110299
 Birkinshaw M. 1979. *MNRAS* 187:847–862
 Birkinshaw M. 1991. in *Physical Cosmology*, eds. A. Blanchard, L. Celnikier, M. Lachi’eze-Rey, J. Tran Thanh Van, Editions Frontieres, Gif sur Yvette, France, p. 177
 Birkinshaw M, Hughes, JP, Arnaud KA. 1991. *ApJ*, 379:466–481
 Birkinshaw M. 1999. *Physics Reports* 310:97–195
 Birkinshaw M, Gull SF, Northover KJE. 1978a. *Nature* 275:40–41
 Birkinshaw M, Gull SF, Northover KJE. 1978b. *MNRAS* 185:245–62
 Birkinshaw M, Hughes JP. 1994. *ApJ* 420:33–43
 Blain AW. 1998. *MNRAS* 297:502–10
 Bond J, Kaiser N, Cole S, Efstathiou G. 1991. *ApJ* 379:440–60
 Bond JR, Myers ST. 1991. in K Sato, ed., *ASSL Vol. 169: Primordial Nucleosynthesis and Evolution of Early Universe* p. 305–23
 Bond JR, Myers ST. 1996. *ApJS* 103:63–79
 Borgani S, Rosati P, Tozzi P, Stanford SA, Eisenhardt PR, et al. 2001. *ApJ* 561:13–21
 Bryan GL. 2000. *ApJ* 544:L1–5
 Burles S, Nollett K, Truran J, Turner M. 1999. *Phys. Rev. Lett.* 82:4176–79
 Burles S, Nollett K, Turner MS. 2001. *ApJ* 552:L1–5
 Burles S, Tytler D. 1998. *ApJ* 499:699–712
 Burles S, Tytler D. 1998. *ApJ* 507:732–44
 Carlstrom JE, Joy M, Grego L, Holder G, Holzapfel WL, et al. 2000. in F Durret, G Gerbal, eds., *Constructing the Universe with Clusters of Galaxies* IAP pp. E43
 Carlstrom JE, Joy M, Grego LE. 1996. *ApJ* 456:L75–78
 Carlstrom JE, Joy MK, Grego L, Holder GP, Holzapfel WL, et al. 2000. *Physica Scripta Volume T* 85:148–55

Carroll S, Press W, Turner E. 1992. *ARA&A* 30:499–542
 Cavaliere A, Danese L, de Zotti G. 1977. *ApJ* 217:6–15
 Cavaliere A, Fusco-Femiano R. 1978. *A&A* 70:677–84
 Cen R. 2001. *ApJ* 546:L77–80
 Challinor A, Lasenby A. 1998. *ApJ* 499:1–6
 Challinor A, Lasenby A. 1999. *ApJ* 510:930–33
 Church SE, Ganga KM, Ade PAR, Holzapfel WH, Mautkopf PD, et al. 1997. *ApJ* 484:523–37
 Colafrancesco S, Mazzotta P, Rephaeli Y, Vittorio N. 1997. *ApJ* 479:1–16
 Cooray AR, Grego L, Holzapfel WL, Joy M, Carlstrom JE. 1998. *AJ* 115:1388–99
 David L, Jones C, Forman W. 1995. *ApJ* 445:578–90
 Dawson KS, Holzapfel WL, Carlstrom JE, Joy M, LaRoque SJ, et al. 2001. *ApJ* 533:L1–4
 de Bernardis P, Ade PAR, Bock JJ, Bond JR, Borrill J, et al. 2000. *Nature* 404:955–59
 De Luca A, Desert FX, Puget JL. 1995. *A&A* 300:335–45
 Desert F, Benoit A, Gaertner S, Bernard J, Coron N, et al. 1998. *New Astronomy* 3:655–69
 Dolgov AD, Hansen SH, Pastor S, Semikoz DV. 2001. *ApJ* 554:74–84
 Evrard A. 1997. *MNRAS* 292:289–97
 Evrard AE, Metzler CA, Navarro JF. 1996. *ApJ* 469:494–507
 Fabbri R. 1981. *Ap&SS* 77:529–37
 Fischer ML, Lange AE. 1993. *ApJ* 419:433–39
 Forman W, Jones C. 1982. *ARA&A* 20:547–85
 Glenn J, Bock JJ, Chattopadhyay G, Edgington SF, Lange AE, et al. 1998. *Proc. SPIE* 3357:326–34
 Grainge K, Grainger WF, Jones ME, Kneissl R, Pooley G, et al. 2001. *MNRAS* 329:890–896
 Grainge K, Jones M, Pooley G, Saunders R, Baker J, et al. 1996. *MNRAS* 278:L17–22
 Grainge K, Jones M, Pooley G, Saunders R, Edge A. 1993. *MNRAS* 265:L57–58
 Grainge K, Jones ME, Pooley G, Saunders R, Edge A, et al. 2000. *MNRAS* submitted:astro-ph/9904165
 Grainger WF, Das R, Grainge K, Jones ME, Kneissl R, et al. 2001. *MNRAS* submitted: astro-ph/0102489
 Grego L, Carlstrom JE, Joy MK, Reese ED, Holder GP, et al. 2000. *ApJ* 539:39–51
 Grego L, Carlstrom JE, Reese ED, Holder GP, Holzapfel WL, et al. 2001. *ApJ* 552:2–14
 Gunn JE. 1978. in *Observational Cosmology Advanced Course* p. 1
 Haiman Z, Mohr JJ, Holder GP. 2001. *ApJ* 553:545–61
 Hanany S, Ade P, Balbi A, Bock J, Borrill J, et al. 2000. *ApJ* 545:L5–9
 Heath DJ. 1977. *MNRAS* 179:351–58
 Herbig T, Lawrence CR, Readhead ACS, Gulkis S. 1995. *ApJ* 449:L5–8
 Holder G, Carlstrom J. 1999. in A de Oliveira-Costa, M Tegmark, eds., *Microwave Foregrounds* San Francisco: ASP– pp. 199–216 astro-ph/9904220
 Holder G, Haiman Z, Mohr JJ. 2001. *ApJ* 560:L111–14
 Holder GP, Carlstrom JE. 2001. *ApJ* 558:515–19
 Holder GP, Carlstrom JE, Evrard AE. 2000. in F Durret, G Gerbal, eds., *Constructing the Universe with Clusters of Galaxies* IAP pp. E45
 Holder GP, Mohr JJ, Carlstrom JE, Evrard EA, Leitch EM. 2000. *ApJ* 544:629–35
 Holzapfel WL, Ade PAR, Church SE, Mautkopf PD, Rephaeli Y, et al. 1997. *ApJ* 481:35–48
 Holzapfel WL, Wilbanks TM, Ade P, Church SE, Fischer M, et al. 1997. *ApJ* 479:17–30
 Hu W, White M. 1997. *ApJ* 479:568–79
 Hughes JP, Birkinshaw M. 1998. *ApJ* 501:1–14
 Itoh N, Kohyama Y, Nozawa S. 1998. *ApJ* 502:7–15
 Jenkins A, Frenk CS, White SDM, Colberg JM, Cole S, et al. 2001. *MNRAS* 321:372–84
 Jones M, Saunders R, Alexander P, Birkinshaw M, Dillon N, et al. 1993. *Nature* 365:320–23
 Jones ME, Edge AC, Grainge K, Grainger WF, Kneissl R, et al. 2001. *MNRAS* submitted:astro-ph/0103046
 Joy M, Laroque S, Grego L, Carlstrom JE, Dawson K, et al. 2001. *ApJ* 551:L1–L4
 Kamionkowski M, Loeb A. 1997. *Phys. Rev. D* 56:4511–13
 Kitayama T, Sasaki S, Suto Y. 1998. *PASJ* 50:1–11
 Kneissl R, Jones ME, Saunders R, Eke VR, Lasenby AN, et al. 2001. *MNRAS* 328:783–94
 Komatsu E, Kitayama T, Suto Y, Hattori M, Kawabe R, et al. 1999. *ApJ* 516:L1–4
 Komatsu E, Matsuo H, Kitayama T, Hattori M, Kawabe R, et al. 2001. *PASJ* 53:57–62
 Korolev VA, Syunyaev RA, Yakubtsev LA. 1986. *Soviet Astronomy Letters* 12:141–147
 Lamarre JM, Giard M, Pointecouteau E, Bernard JP, Serra G, et al. 1998. *ApJ* 507:L5–8
 LaRoque SJ, Carlstrom JE, Reese ED, Holder GP, Holzapfel WL, et al. 2001. *ApJ*. Submitted. astro-ph/0204134
 Loeb A, Mao S. 1994. *ApJ* 435:L109–12
 Loeb A, Refregier A. 1997. *ApJ* 476:L59–62
 Markevitch M, Blumenthal GR, Forman W, Jones C, Sunyaev RA. 1994. *ApJ* 426:1–13
 Markevitch M, Ponman TJ, Nulsen PEJ, Bautz MW, Burke DJ, et al. 2000. *ApJ* 541:542–49

- Mason BS. 1999. *An Improved Measurement of the Hubble Constant Using the Sunyaev-Zel'dovich Effect* Ph.D. thesis University of Pennsylvania
- Mason BS, Myers ST, Readhead ACS. 2001. *ApJ* 555:L11-L15
- Mauskopf PD, Ade PAR, Allen SW, Church SE, Edge AC, et al. 2000a. *ApJ* 538:505
- Mauskopf PD, Rownd BK, Edgington SF, Hristov VV, Mainzer AK, et al. 2000b. in *Imaging at Radio through Submillimeter Wavelengths. Edited by Jeff Mangum. Publisher: The Astronomical Society of the Pacific, Conference Series, San Francisco* p. E46
- Miller AD, Caldwell R, Devlin MJ, Dorwart WB, Herbig T, et al. 1999. *ApJ* 524:L1-4
- Miralda-Escude J, Babul A. 1995. *ApJ* 449:18-27
- Mohr J, Mathiesen B, Evrard A. 1999. *ApJ* 517:627-49
- Molnar SM, Birkinshaw M. 1999. *ApJ* 523:78-86
- Mushotzky RF, Scharf CA. 1997. *ApJ* 482:L13-L16
- Myers ST, Baker JE, Readhead ACS, Leitch EM, Herbig T. 1997. *ApJ* 485:1-21
- Netterfield CB, Ade PAR, Bock JJ, Bond JR, Borrill J, et al. 2002. *ApJ* submitted:astro-ph/0104460
- Neumann DM, Bohringer H. 1997. *MNRAS* 289:123-35
- Nevalainen J, Markevitch M, Forman W. 2000. *ApJ* 536:73-78
- Nollett KM, Burles S. 2000. *Phys. Rev. D* 61:123505
- Nozawa S, Itoh N, Kohyama Y. 1998a. *ApJ* 508:17-24
- Nozawa S, Itoh N, Kohyama Y. 1998b. *ApJ* 507:530-57
- Oukbir J, Bartlett JG, Blanchard A. 1997. *A&A* 320:365-77
- Padin S, Cartwright JK, Mason BS, Pearson, TJ, Readhead ACS, et al. 2000. *ApJ* 549:L1-L5
- Patel SK, Joy M, Carlstrom JE, Holder GP, Reese ED, et al. 2000. *ApJ* 541:37-48
- Peebles P. 1980. *The Large Scale Structure of the Universe* Princeton, NJ: Princeton University Press
- Peebles P. 1994. *Physical Cosmology* Princeton, NJ: Princeton University Press
- Perlmutter S, Aldering G, Goldhaber G, Knop R, Nugent P, et al. 1999. *ApJ* 517:565-86
- Phillips PR. 1995. *ApJ* 455:419-20
- Pointecouteau E, Giard M, Benoit A, Désert FX, Aghanim N, et al. 1999. *ApJ* 519:L115-18
- Pointecouteau E, Giard M, Benoit A, Désert FX, Bernard JP, Corón N, Lamarre JM. 2001. *ApJ* 552:42-48
- Ponman TJ, Cannon DB, Navarro, JF. 1999. *Nature* 397:135-137
- Pospieszalski MW, Lakatos WJ, Nguyen LD, Lui M, Liu T, et al. 1995. *IEEE MTT-S Int. Microwave Symp.*, 1121-1124
- Press W, Schechter P. 1974. *ApJ* 187:425-38
- Pryke C, Halverson NW, Leitch EM, Kovac J, Carlstrom JE, et al. 2002. *ApJ* 568. astro-ph/0104490
- Reese ED, Carlstrom JE, Joy M, Mohr JJ, Grego L, et al. 2002. *ApJ*. In press. astro-ph/020535
- Reese ED, Mohr JJ, Carlstrom JE, Joy M, Grego L, et al. 2000. *ApJ* 533:38-49
- Rephaeli Y. 1995. *ARA&A* 33:541-80
- Rephaeli Y, Yankovitch D. 1997. *ApJ* 481:L55-L58
- Riess AG, Filippenko AV, Challis P, Clocchiattia A, Diercks A, et al. 1998. *AJ* 116:1009-38
- Saunders R, Kneissl R, Grainge K, Jones ME, Maggi A, et al. 2000. *MNRAS* submitted:astro-ph/9904168
- Sazonov SY, Sunyaev RA. 1998a. *ApJ* 508:1-5
- Sazonov SY, Sunyaev RA. 1998b. *Astronomy Letters* 24:553-67
- Sazonov SY, Sunyaev RA. 1999. *MNRAS* 310:765-72
- Sheth RK, Mo HJ, Tormen G. 2001. *MNRAS* 323:1-12
- Silk J, White SDM. 1978. *ApJ* 226:L103-6
- Smail I, Ivison RJ, Blain AW. 1997. *ApJ* 490:L5-8
- Springel V, White M, Hernquist L. 2001. *ApJ* 549:681-87
- Squires G, Kaiser N. 1996. *ApJ* 473:65-80
- Squires G, Neumann DM, Kaiser N, Arnaud M, Babul A, et al. 1997. *ApJ* 482:648-58
- Stebbins A. 1997. *preprint*. astro-ph/9709065
- Stompor R, Abrob M, Ade P, Balbi A, Barbosa D, et al. 2001. *ApJ* 561:L7-10
- Subrahmanyan R, Kesteven MJ, Ekers RD, Sinclair M, Silk J. 2000. *MNRAS* 315:808-22
- Sulkanen ME. 1999. *ApJ* 522:59-65
- Sunyaev RA, Zel'dovich YB. 1970. *Comments Astrophys. Space Phys.* 2:66-74
- Sunyaev RA, Zel'dovich YB. 1972. *Comments Astrophys. Space Phys.* 4:173-78
- Sunyaev RA, Zel'dovich YB. 1980a. *ARA&A* 18:537-60
- Sunyaev RA, Zel'dovich YB. 1980b. *MNRAS* 190:413-20
- Tamura T, Kaastra JS, Peterson JR, Paerels FBS, Mittaz JPD, et al. 2001. *A&A* 365:L87-92
- Thompson AR, Moran JM, Swenson GW. 2001. *Interferometry and Synthesis in Radio Astronomy* New York, NY: Wiley-Interscience
- Tsuboi M, Miyazaki A, Kasuga T, Matsuo H,

- Kuno N. 1998. *Proc. Astron. Soc. Japan* 50:169-73
- Tucker W, Blanco P, Rappoport S, David L, Fabricant D, et al. 1998. *ApJ* 496:L5-8
- Udomprasert PS, Mason BS, Readhead ACS. 2000. in F Durret, G Gerbal, eds., *Constructing the Universe with Clusters of Galaxies* IAP pp. E48
- Viana P, Liddle A. 1999. *MNRAS* 303:535-45
- Weller J, Bat-tye RA, Kneissl R. 2001. *Phys. Rev. Lett.* submitted:astro-ph/0110353
- White DA, Fabian AC. 1995. *MNRAS* 273:72-84
- White S, Navarro J, Evrard A, Frenk C. 1993. *Nature* 366:429-33
- Wright EL. 1979. *ApJ* 232:348-51
- Wu X, Fang L. 1997. *ApJ* 483:62-67